Mathematical Biosciences and Engineering

http://www.aimspress.com/journal/mbe

MBE, 20(6): 11281–11312.
DOI: 10.3934/mbe.2023500
Received: 07 February 2023
Revised: 09 April 2023
Accepted: 17 April 2023
Published: 26 April 2023

Research article

Computational modeling of fractional COVID-19 model by Haar wavelet collocation methods with real data

Rahat Zarin[1], Usa Wannasingha Humphries[1], Amir Khan[2] and Aeshah A. Raezah[3,*]

[1] Department of Mathematics, Faculty of Science, King Mongkut's University of Technology, Thonburi (KMUTT), 126 Pracha-Uthit Road, Bang Mod, Thrung Khru, Bangkok 10140, Thailand

[2] Department of Mathematics and Statistics, University of Swat, Khyber Pakhtunkhawa, Pakistan

[3] Department of Mathematics, Faculty of Science, King Khalid University, Abha 62529, Saudi Arabia

* **Correspondence:** Email: aalraezh@kku.edu.sa.

Abstract: This study explores the use of numerical simulations to model the spread of the Omicron variant of the SARS-CoV-2 virus using fractional-order COVID-19 models and Haar wavelet collocation methods. The fractional order COVID-19 model considers various factors that affect the virus's transmission, and the Haar wavelet collocation method offers a precise and efficient solution to the fractional derivatives used in the model. The simulation results yield crucial insights into the Omicron variant's spread, providing valuable information to public health policies and strategies designed to mitigate its impact. This study marks a significant advancement in comprehending the COVID-19 pandemic's dynamics and the emergence of its variants. The COVID-19 epidemic model is reworked utilizing fractional derivatives in the Caputo sense, and the model's existence and uniqueness are established by considering fixed point theory results. Sensitivity analysis is conducted on the model to identify the parameter with the highest sensitivity. For numerical treatment and simulations, we apply the Haar wavelet collocation method. Parameter estimation for the recorded COVID-19 cases in India from 13 July 2021 to 25 August 2021 has been presented.

Keywords: fractional modeling; Haar wavelet; COVID-19; reproduction number; epidemic model; parameter estimation

1. Introduction

The SARS-CoV-2 virus triggered a pandemic worldwide. SARS-CoV-2, a spike protein virus, is the pathogen that causes widespread Coronavirus infections. Coronaviruses make up a broad family of viruses. The first serious disease attributed to a coronavirus is the severe acute respiratory syndrome

(SARS) an epidemic that began in China in 2003. Saudi Arabia was home to a second epidemic, middle east respiratory syndrome (MERS), first reported in 2012 [1]. In December 2019, Wuhan, China, announced a SARS coronavirus 2 outbreak (COVID-19). The World Health Organization (WHO) classified COVID-19 as a worldwide epidemic in March 2020. As of 8 January 2023, over 659 million cases have been confirmed worldwide, resulting in over 6.6 million deaths [2]. Typically, The disease is contracted through exposure to infected respiratory droplets from breathing, coughing, sneezing, and talking [3–7]. The disease is transmissible through the air, according to further research [8–13]. The risk of infection is also present when contact is made with objects that are contaminated with Covid-19. It has been observed that COVID-19 can cause a coughing fit, pain in the muscles, vertigo, high temperature, an inability to smell, throat irritation, weakness, and nasal congestion after 2–14 days of incubation of the virus.

The Omicron variant has been characterized by its high transmissibility and numerous mutations, which have raised concerns about its potential to evade immunity conferred by vaccines or prior infection. In response, India has implemented measures such as booster doses and vaccine mix-and-match regimens to enhance protection against the new variant. Furthermore, the Indian government has also imposed stricter quarantine rules for international travelers, particularly those arriving from countries with high Omicron prevalence. Despite these efforts, challenges remain, particularly in remote or under-resourced areas where healthcare infrastructure and resources may be limited. Additionally, the emergence of new variants underscores the need for ongoing surveillance and research to better understand the virus and its behavior. To that end, India has continued to invest in genomic sequencing efforts, which have played a crucial role in tracking the spread of different variants. As India continues to navigate the ongoing COVID-19 pandemic, the situation with Omicron remains dynamic, and it is important to remain vigilant and adaptable in the face of new developments.

Globally, the COVID-19 pandemic continues to pose a serious threat to public health. Three recent publications offer insight into the crucial elements that ought to direct disease containment efforts. A risk assessment of COVID-19 reappearance in connection to SARS-CoV-2 mutations and vaccine success is provided by Krueger et al. [14] in 2022. They place a strong emphasis on the value of immunization and the necessity of ongoing surveillance of the disease's spread. The necessity for a coordinated European response to the omicron version of COVID-19 is highlighted by Calero Valdez et al. [15] in 2022. To slow the spread of the variation and prevent a spike in cases, the authors contend that concerted action is required. In the meanwhile, Markovi et al. [16] (2021) provide evidence that socio-demographic and health characteristics are important contributors to the spread of the COVID-19 outbreak and recommend that vaccination regimens should consider these aspects for efficient disease control. Collectively, these papers highlight the significance of a thorough, evidence-based strategy for COVID-19 regulation that considers both individual and population-level determinants.

Dynamical systems have become increasingly complex, and fractional calculus (FC) has become an increasingly useful tool. The process of differentiation and integration in FC is generalized to non-integer orders. FC has been applied to research in a variety of fields. In order to gain a deeper understanding of a disease, fractional order differential equations (FODs) are used. For various diseases, mathematical models have been formulated and studied, for example, [17–22]. In order to overcome the deficiencies of the ordinary operator, fractional order derivatives have been developed [23]. Riemann-Liouville proposed the concept of the fractional derivative (FD). Caputo later reformulated and improved FD. The formula of Caputo FD is based on the singular power-law kernel. FDs are

commonly used to study real problems, but they often yield singularities that are dissatisfactory. Following decades, and for this reason, Caputo-Fabrizio (CF) operators is created through nonsingular kernels [24]. CF, however, has a kernel locality problem. As a solution to this shortcoming, Atangana and Baleanu (AB) [25] proposed Mittag-Leffler kernels as a novel type of FD.

Several works [26–28] have proposed fractional operators with singular and nonsingular kernels, and recent publications such as [29–35] explore the research related to these topics and their applications. Additionally, mathematical modeling studies have recently emerged to address social issues, such as criminal activity, using FC. In order to convert the proposed fractional-order crime transmission model to the delayed model and account for the lag between the crime and judgment, Bansal et al. [36] established the time-delay coefficient. Pritam et al. [37] studied a fractional-order mathematical model of crime transmission that includes the memory property inherited from the previous impact of the input while predicting the crime growth rate in analyzing crime congestion. By using the actual initial conditions for the subgroups of the USA, Partohaghighi et al. [38] designed and compared the fractional-order crime systems for the first time using the Atangana-Baleanu-Caputo (ABC), Caputo, and Caputo-Fabrizio derivatives and to obtain approximate solutions to the proposed models, they developed some numerical methods. Rahman et al. [39] presented a study on the dynamics of a fractional mathematical model of serial killing under the Mittag-Leffler kernel, [39] discovered the approximate solution and numerically simulated it for multiple control techniques in various fractional orders using the iterative fractional-order Adams-Bashforth approach.

Haar wavelet numerical methods are a family of mathematical techniques used to solve differential equations with fractional derivatives. These methods are based on the Haar wavelet, a simple wavelet function that provides a piecewise constant approximation of a signal. The Haar wavelet is well suited for the numerical solution of fractional differential equations due to its simplicity, local support, and orthogonality. One of the main advantages of Haar wavelet numerical methods is their ability to provide efficient and accurate solutions to fractional differential equations. Unlike traditional numerical methods, which can be time-consuming and prone to errors when solving problems with fractional derivatives, Haar wavelet methods are computationally efficient and produce accurate solutions. Haar wavelet numerical methods have been applied to a wide range of problems in various fields, including physics, engineering, and finance. For example, they have been used to study the diffusion of heat in porous media, to model the dynamic behavior of financial markets, and to analyze the spread of infectious diseases. Haar wavelet numerical methods have gained significant attention in the past few years for solving problems associated with the COVID-19 pandemic. These methods have been employed to model the virus's propagation over time while accounting for the multiple factors influencing its transmission. Through these studies, useful information has been obtained regarding the pandemic's dynamics, its evolution, and its impact, which has helped in developing public health policies and strategies aimed at managing its spread.

The use of Haar wavelet numerical methods has gained popularity in various fields, including numerical analysis, image processing, quantum field theory, and statistics. Haar wavelets have been applied in communication, physics research, differential equations, and nonlinear problems [40]. They are preferred among all wavelet families because they are the simplest wavelet family that comprises pairs of piecewise constant functions. Additionally, they can be integrated analytically at random times. Recent research has employed Haar wavelets to solve various fractional-order mathematical models [41, 42]. The Haar wavelet technique is not only fast but also more stable, making it an excel-

lent option for numerical computation.

The innovative aspects of the paper include the application of Haar wavelet collocation methods and fractional order COVID-19 models to the simulation of the Omicron variant of the SARS-CoV-2 virus and the dynamics of the COVID-19 pandemic as well as the evolution of its variants. The results of the study can help shape public health policies and actions targeted at reducing its impact since they provide a more precise and effective solution to the fractional derivatives employed in the model. The importance of this work in furthering our understanding of COVID-19 is increased by the inclusion of parameter estimates and stability analysis. The remainder of the article is structured as follows: In Section 2, the basic concepts of the fractional differential, integral operator, and Haar wavelets have been presented. In Section 3, the fractional extension of the model has been formulated, and the equilibrium point and threshold number have been calculated. In Section 4, the existence and uniqueness of the solution of the model have been established and the numerical scheme is described. Section 5 provides parameter estimation for the COVID-19 reported data in India from 13 July to 25 August 2021. The sensitivity analysis of the model is cared out in Section 6. The numerical scheme and graphical results are presented in Section 7. Conclusions and future research direction have been offered in Section 8.

2. Preliminaries

In recent years, significant progress has been made in the definition of fractional derivatives. This progress has been documented in various sources, including [30, 31, 43–45]. The updated definitions encompass non-singular kernel derivatives, as well as the Riemann-Liouville fractional derivative without a singular kernel and the two-parameter derivative with non-singular and non-local kernels. Out of these, the following two definitions are widely accepted in the field:

Definition 1. *Riemann-Liouville's definition characterizes the fractional derivative of $\mathcal{F}$ with order δ. The definition can be expressed as follows:*

$$\mathbb{D}_*^{\delta}\mathcal{F}(t) = \begin{cases} \frac{1}{\Gamma(s-\delta)}\left(\frac{d}{dt}\right)^s \int_0^t \frac{\mathcal{F}(\nu)}{(t-\nu)^{\delta-s+1}}d\nu, & 0 \le s-1 < \delta < s, \quad s \in \mathbb{N}, \\ (d/dt)^s\mathcal{F}(t), & \delta = s, \quad s \in \mathbb{N}. \end{cases} \tag{2.1}$$

Definition 2. *The function $\mathcal{F}$ can be differentiated with respect to the fractional order δ using the Caputo fractional derivative, which is defined in the following manner:*

$$\mathbb{D}_*^{\delta}\mathcal{F}(t) = \begin{cases} \frac{1}{\Gamma(s-\delta)} \int_0^t \frac{(d/d\nu)^s\mathcal{F}(\nu)}{(t-\nu)^{\delta-s+1}}d\nu, & 0 \le s-1 < \delta < s, \quad s \in \mathbb{N}, \\ (d/dt)^s\mathcal{F}(t), & \delta = s, \quad s \in \mathbb{N}. \end{cases} \tag{2.2}$$

The study also employs the RL representation of the fractional integral operator $\mathbb{D}_*^{-\delta}$ with order δ. This operator can be defined in the following manner:

$$\mathbb{D}_*^{-\delta}\mathcal{F}(t) = \frac{1}{\Gamma(\delta)}\int_0^t \mathcal{F}(\nu)(t-\nu)^{\delta-1}d\nu \tag{2.3}$$

2.1. Haar wavelets

According to [46, 47], the mother Haar wavelet function (on the real line) is denoted as $\psi(t)$, while the Haar scaling function is represented by $\tilde{\psi}_0(t)$:

$$\psi(t) = \begin{cases} 1, & \text{if } t \in \left[0, \frac{1}{2}\right), \\ -1, & \text{if } t \in \left[\frac{1}{2}, 1\right), \\ 0, & \text{elsewhere,} \end{cases} \tag{2.4}$$

$$\tilde{\psi}_0(t) = 1, \text{ if } t \in [0, 1). \tag{2.5}$$

Multiresolution analysis generates multiple Haar wavelets on the interval $[0, 1)$, which can be denoted as $\tilde{\psi}_m(t)$. As a consequence, the following relationship holds:

$$\tilde{\psi}_m(t) = 2^{j/2}\psi\left(2^j t - p\right), m = 1, 2, \ldots; \tag{2.6}$$

where $m = 2^j + p : p = 0, 1, \ldots, 2^j - 1; j = 0, 1, \ldots$. Further, we can translate the Haar functions on $u - 1 \leq t < u$ as

$$\tilde{\psi}_{u,m}(t) = \tilde{\psi}_m(t + 1 - u), m = 0, 1, 2, \ldots, \quad u = 1, 2, \ldots, \varrho, \quad \varrho \in \mathbb{N}. \tag{2.7}$$

According to [47], the sequence $\left\{\tilde{\psi}_m(t)\right\}_{m=0}^{\infty}$ forms a complete orthonormal system in $\mathcal{L}^2[0, 1)$, while the sequence $\left\{\tilde{\psi}_{u,m}(t)\right\}_{m=0}^{\infty}, u = 1, 2, \ldots, \varrho$, forms a complete orthonormal system in $\mathcal{L}^2[0, \varrho)$. This implies that any function $\mathcal{F}(t)$ belonging to $\mathcal{L}^2[0, \varrho)$ can be expressed as a series of Haar orthonormal basis functions.

$$\mathcal{F}(t) = \sum_{u=1}^{\varrho} \sum_{m=0}^{\infty} \mathcal{G}_{u,m} \tilde{\psi}_{u,m}(t). \tag{2.8}$$

Additionally, after truncating this series $\mathcal{F}(t)$, we obtain the equivalent approximation $y_p(t)$ of $\mathcal{F}(t)$ as

$$\mathcal{F}(t) \approx y_p(t) = \sum_{u=1}^{\varrho} \sum_{m=0}^{p-1} \mathcal{G}_{u,m} \tilde{\psi}_{u,m}(t) = B^T_{\varrho p \times 1} \tilde{\psi}_{\varrho p \times 1}(t), \tag{2.9}$$

where the coefficients $\mathcal{G}_{u,m}$ can be expressed by inner product

$$\begin{aligned} &\left\langle \mathcal{F}(t), \tilde{\psi}_{u,m}(t) \right\rangle = \int_{u-1}^{u} \mathcal{F}(t) \tilde{\psi}_{u,m}(t) dt, \quad m = 1, 2, \ldots, (p-1), u = 1, 2, \ldots, \varrho, \\ &B_{\varrho p \times 1} = \left[\mathcal{G}_{1,0}, \ldots, \mathcal{G}_{1,p-1}, \mathcal{G}_{2,0}, \ldots, \mathcal{G}_{2,p-1}, \ldots, \mathcal{G}_{\varrho,0}, \ldots, \mathcal{G}_{\varrho,p-1}\right]^T, \\ &\tilde{\psi}_{\varrho p \times 1} = \left[\tilde{\psi}_{1,0}, \ldots, \tilde{\psi}_{1,p-1}, \tilde{\psi}_{2,0}, \ldots, \tilde{\psi}_{2,p-1}, \ldots, \tilde{\psi}_{\varrho,0}, \ldots, \tilde{\psi}_{\varrho,p-1}\right]^T, \end{aligned} \tag{2.10}$$

and superscript T indicates the transpose of a matrix.

3. Mathematical model

Mathematical modeling plays a crucial role in understanding and predicting the spread of infectious diseases. By using mathematical equations and algorithms, researchers can simulate the behavior of

diseases and their transmission within populations. This allows them to make predictions about the future spread of the disease and to test various intervention strategies. Mathematical models can also provide valuable insights into the basic mechanisms of disease transmission, helping to identify risk factors and to inform public health policies. However, it is important to note that the accuracy of these models depends on the quality of data input and the assumptions made in the model, and they should always be used in conjunction with other sources of information. Considering the work of [7, 11], the model applied takes the form of the following ODEs:

$$\begin{cases} \dfrac{d\mathbb{S}(t)}{dt} = B - \theta\mathbb{S}(t)\mathbb{I}(t)(1+\tau\mathbb{I}(t)) - (\varepsilon_1+\rho+\eta)\mathbb{S}(t), \\ \dfrac{d\mathbb{E}(t)}{dt} = \theta\mathbb{S}(t)\mathbb{I}(t)(1+\tau\mathbb{I}(t)) - (\varepsilon_2+\rho+\varphi)\mathbb{E}(t), \\ \dfrac{d\mathbb{I}(t)}{dt} = \varphi\mathbb{E}(t) - (\lambda+\epsilon+\rho+\varepsilon_3)\mathbb{I}(t), \\ \dfrac{d\mathbb{Q}(t)}{dt} = \varepsilon_1\mathbb{S}(t) + \varepsilon_2\mathbb{E}(t) + \varepsilon_3\mathbb{I}(t) - (\rho+\sigma)\mathbb{Q}(t), \\ \dfrac{d\mathbb{R}(t)}{dt} = \eta\mathbb{S}(t) + \sigma\mathbb{Q}(t) + \lambda\mathbb{I}(t) - \rho\mathbb{R}(t), \\ \mathbb{S}(t)\geq 0, \quad \mathbb{E}(t)\geq 0, \quad \mathbb{I}(t)\geq 0, \quad \mathbb{Q}(t)\geq 0, \quad \mathbb{R}(t)\geq 0. \end{cases} \tag{3.1}$$

where,

$$\mathbb{N}(t) = \mathbb{S}(t) + \mathbb{E}(t) + \mathbb{I}(t) + \mathbb{Q}(t) + \mathbb{R}(t).$$

According to the five categories, the total population at time t is represented by $\mathbb{N}(t)$ in model (3.1). The individuals who are susceptible to infection are designated as $\mathbb{S}(t)$; exposed individuals are designated as $\mathbb{E}(t)$; infectious individuals are designated as $\mathbb{I}(t)$; and quarantined individuals are designated as $\mathbb{Q}(t)$; and recovered individuals are designated as $\mathbb{R}(t)$. The parameters θ and τ are positive constants, whereas B is the constant birth rate, θ is the coefficient of disease transmission,ρ is the natural death rate, andϵ is the mortality rate from infectious disease in humans and $\varphi, \lambda, \varepsilon_3, \varepsilon_2, \varepsilon_1, \sigma$ are the state transition rates. The term η refers to the transmission rate from the class of persons who are immune system-strong to those who are susceptible to it.

3.1. Formulation of fractional model

The Caputo fractional derivative offers a significant advantage over classical models in the context of COVID-19 modeling by allowing for a more accurate representation of complex phenomena, such as the long-lasting effects of the disease on patients. Unlike classical models that assume instant recovery after an infection, Caputo fractional derivatives account for the memory effect of the disease, which can persist even after recovery, enabling more precise predictions and better decision-making regarding healthcare resource allocation and pandemic control measures. Additionally, using the Caputo derivative often requires less computational resources and less data, making it a more cost-effective solution in disease modeling. Furthermore, time memory effect can be found in most natural phenomena, such as epidemiological dynamics. Model (3.1) is expressed in integral form as:

$$\begin{cases} \dfrac{d\mathbb{S}(t)}{dt} = \displaystyle\int_{t_0}^{t} \varsigma(t-\vartheta)\left[B - \theta\mathbb{S}(t)\mathbb{I}(t)(1+\tau\mathbb{I}(t)) - (\varepsilon_1+\rho+\eta)\mathbb{S}(t)\right] d\vartheta, \\ \dfrac{d\mathbb{E}(t)}{dt} = \displaystyle\int_{t_0}^{t} \varsigma(t-\vartheta)\left[\theta\mathbb{S}(t)\mathbb{I}(t)(1+\tau\mathbb{I}(t)) - (\varepsilon_2+\rho+\varphi)\mathbb{E}(t)\right] d\vartheta, \\ \dfrac{d\mathbb{I}(t)}{dt} = \displaystyle\int_{t_0}^{t} \varsigma(t-\vartheta)\left[\varphi\mathbb{E}(t) - (\lambda+\epsilon+\rho+\varepsilon_3)\mathbb{I}(t)\right] d\vartheta, \\ \dfrac{d\mathbb{Q}(t)}{dt} = \displaystyle\int_{t_0}^{t} \varsigma(t-\vartheta)\left[\varepsilon_1\mathbb{S}(t) + \varepsilon_2\mathbb{E}(t) + \varepsilon_3\mathbb{I}(t) - (\rho+\sigma)\mathbb{Q}(t)\right] d\vartheta, \\ \dfrac{d\mathbb{R}(t)}{dt} = \displaystyle\int_{t_0}^{t} \varsigma(t-\vartheta)\left[\eta\mathbb{S}(t) + \sigma\mathbb{Q}(t) + \lambda\mathbb{I}(t) - \rho\mathbb{R}(t)\right] d\vartheta. \end{cases} \tag{3.2}$$

Incorporating the Caputo derivative we get,

$$\begin{cases} {}^{C}D_t^{\delta-1}\left[\dfrac{d\mathbb{S}(t)}{dt}\right] = {}^{C}D_t^{\delta-1} I^{-(\delta-1)}\left[B - \theta\mathbb{S}(t)\mathbb{I}(t)(1+\tau\mathbb{I}(t)) - (\varepsilon_1+\rho+\eta)\mathbb{S}(t)\right], \\ {}^{C}D_t^{\delta-1}\left[\dfrac{d\mathbb{E}(t)}{dt}\right] = {}^{C}D_t^{\delta-1} I^{-(\delta-1)}\left[\theta\mathbb{S}(t)\mathbb{I}(t)(1+\tau\mathbb{I}(t)) - (\varepsilon_2+\rho+\varphi)\mathbb{E}(t)\right], \\ {}^{C}D_t^{\delta-1}\left[\dfrac{d\mathbb{I}(t)}{dt}\right] = {}^{C}D_t^{\delta-1} I^{-(\delta-1)}\left[\varphi\mathbb{E}(t) - (\lambda+\epsilon+\rho+\varepsilon_3)\mathbb{I}(t)\right], \\ {}^{C}D_t^{\delta-1}\left[\dfrac{d\mathbb{Q}(t)}{dt}\right] = {}^{C}D_t^{\delta-1} I^{-(\delta-1)}\left[\varepsilon_1\mathbb{S}(t) + \varepsilon_2\mathbb{E}(t) + \varepsilon_3\mathbb{I}(t) - (\rho+\sigma)\mathbb{Q}(t)\right], \\ {}^{C}D_t^{\delta-1}\left[\dfrac{d\mathbb{R}(t)}{dt}\right] = {}^{C}D_t^{\delta-1} I^{-(\delta-1)}\left[\eta\mathbb{S}(t) + \sigma\mathbb{Q}(t) + \lambda\mathbb{I}(t) - \rho\mathbb{R}(t)\right]. \end{cases} \tag{3.3}$$

After calculations, we reaches

$$\begin{cases} {}^{C}D_t^{\delta}\mathbb{S}(t) = B - \theta\mathbb{S}(t)\mathbb{I}(t)(1+\tau\mathbb{I}(t)) - (\varepsilon_1+\rho+\eta)\mathbb{S}(t), \\ {}^{C}D_t^{\delta}\mathbb{E}(t) = \theta\mathbb{S}(t)\mathbb{I}(t)(1+\tau\mathbb{I}(t)) - (\varepsilon_2+\rho+\varphi)\mathbb{E}(t), \\ {}^{C}D_t^{\delta}\mathbb{I}(t) = \varphi\mathbb{E}(t) - (\lambda+\epsilon+\rho+\varepsilon_3)\mathbb{I}(t), \\ {}^{C}D_t^{\delta}\mathbb{Q}(t) = \varepsilon_1\mathbb{S}(t) + \varepsilon_2\mathbb{E}(t) + \varepsilon_3\mathbb{I}(t) - (\rho+\sigma)\mathbb{Q}(t), \\ {}^{C}D_t^{\delta}\mathbb{R}(t) = \eta\mathbb{S}(t) + \sigma\mathbb{Q}(t) + \lambda\mathbb{I}(t) - \rho\mathbb{R}(t). \end{cases} \tag{3.4}$$

3.2. Equilibrium point and threshold number R_0

A crucial element of epidemiological modeling is the basic reproductive number R_0, which expresses the typical number of secondary infections brought on by a single infected person in a population that is fully susceptible. In the context of epidemiological modeling, R_0 offers numerous benefits:

- **It provides a clear measure of the transmissibility of a disease:** A high R_0 indicates that a disease is easily transmitted, while a low R_0 suggests that it is less contagious.
- **It helps to predict the potential spread of an outbreak:** By estimating R_0, epidemiologists can predict the potential size and duration of an outbreak and identify the most effective control measures.

- **It can be used to evaluate the effectiveness of interventions:** By comparing the R_0 before and after an intervention, such as the implementation of a vaccine or quarantine measures, epidemiologists can determine the effectiveness of the intervention in reducing transmission.
- **It can be used to identify the critical control points:** R_0 can be used to identify the critical points in the transmission of an infection, such as the number of infected individuals in a population.
- **It can be used to predict the herd immunity threshold:** The herd immunity threshold is the proportion of the population that needs to be immune to a disease in order to achieve herd immunity. R_0 helps to predict the herd immunity threshold and thus the overall effectiveness of vaccination programs.

The DFE of the model (3.4) is denoted by $E^0(\mathbb{S}_0, 0, 0, \mathbb{Q}_0, \mathbb{R}_0)$, where

$$\mathbb{S}_0 = \frac{B}{\eta + \rho + \varepsilon_1}, \quad \mathbb{Q}_0 = \frac{\varepsilon_1 \mathbb{S}_0}{\rho + \tau}, \quad \mathbb{R}_0 = \frac{\eta \mathbb{S}_0 + \tau \mathbb{Q}_0}{\rho}.$$

Our proposed model is split in two matrices [48].

$$\tilde{U} = \begin{bmatrix} 0 & \theta \mathbb{S}_0 \\ 0 & 0 \end{bmatrix}, \ \tilde{V} = \begin{bmatrix} \varphi + \rho + \varepsilon_2 & 0 \\ -\varphi & \rho + \epsilon + \lambda + \varepsilon_3 \end{bmatrix},$$

$$\tilde{V}^{-1} = \frac{1}{(\varphi + \rho + \varepsilon_2)(\rho + \epsilon + \lambda + \varepsilon_3)} \begin{bmatrix} \rho + \epsilon + \lambda + \varepsilon_3 & 0 \\ \varphi & \varphi + \rho + \varepsilon_2 \end{bmatrix},$$

$$\tilde{U}\tilde{V}^{-1} = \begin{bmatrix} \frac{\theta \mathbb{S}_0 \varphi}{(\varphi+\rho+\varepsilon_2)(\rho+\epsilon+\lambda+\varepsilon_3)} & \frac{\theta \mathbb{S}_0}{\rho+\epsilon+\lambda+\varepsilon_3} \\ 0 & 0 \end{bmatrix}.$$

Hence

$$R_0 = \frac{\varphi \theta B}{(\eta + \rho + \varepsilon_1)(\varphi + \rho + \varepsilon_2)(\rho + \epsilon + \lambda + \varepsilon_3)}.$$

4. Existence and uniqueness

The existence and uniqueness of a solution to a mathematical problem is a fundamental concept in many areas of mathematics. In order for a solution to exist, the problem must have at least one solution that satisfies all the given conditions. Uniqueness, on the other hand, refers to the fact that there is only one solution to the problem that satisfies all the given conditions. This is important because it means that any method used to solve the problem will always give the same answer. In many cases, the existence and uniqueness of a solution can be proven through the use of mathematical theorems and techniques such as the existence and uniqueness theorem.

In this section, we describe the existence, uniqueness, and solution of the system (3.4) using the Caputo operator. We assume that the Banach space $\mathcal{A}(Y)$ is a continuous real-valued function with the sup-norm property on $J = [0, b]$, and that $Y = [0, \kappa]$ and $P = \mathcal{A}(Y) \times \mathcal{A}(Y) \times \mathcal{A}(Y) \times \mathcal{A}(Y) \times \mathcal{A}(Y)$ has the norm $\|(\mathbb{S}, \mathbb{E}, \mathbb{Q}, \mathbb{I}, \mathbb{R})\| = \|\mathbb{S}\| + \|\mathbb{E}\| + \|\mathbb{Q}\| + \|\mathbb{I}\| + \|\mathbb{R}\|$. Here, $\|\mathbb{S}\|$, $\|\mathbb{E}\|$, $\|\mathbb{Q}\|$, $\|\mathbb{I}\|$, and $\|\mathbb{R}\|$ are defined as $\sup_{t \in Y} |\mathbb{S}(t)|$, $\sup_{t \in Y} |\mathbb{E}(t)|$, $\sup_{t \in Y} |\mathbb{Q}(t)|$, $\sup_{t \in Y} |\mathbb{I}(t)|$, and $\sup_{t \in Y} |\mathbb{R}(t)|$, respectively. Using the Caputo

fractional integral operator on both sides of (3.4), we obtain the following equation:

$$\begin{cases} \mathbb{S}(t)-\mathbb{S}(0) = {}^{C}\mathbb{D}^{\delta}_{0,t}\mathbb{S}(t)\left\{B-\theta\mathbb{S}\mathbb{I}(1+\tau\mathbb{I})-(\varepsilon_1+\rho+\eta)\mathbb{S}(t)\right\}, \\ \mathbb{E}(t)-\mathbb{E}(0) = {}^{C}\mathbb{D}^{\delta}_{0,t}\mathbb{E}(t)\left\{\theta\mathbb{S}\mathbb{I}(1+\tau\mathbb{I})-(\varepsilon_2+\rho+\varphi)\mathbb{E}(t)\right\}, \\ \mathbb{I}(t)-\mathbb{I}(0) = {}^{C}\mathbb{D}^{\delta}_{0,t}\mathbb{I}(t)\left\{\varphi\mathbb{E}(t)-(\lambda+\epsilon+\rho+\varepsilon_3)\mathbb{I}(t)\right\}, \\ \mathbb{Q}(t)-\mathbb{Q}(0) = {}^{C}\mathbb{D}^{\delta}_{0,t}\mathbb{Q}(t)\left\{\varepsilon_1\mathbb{S}(t)+\varepsilon_2\mathbb{E}(t)+\varepsilon_3\mathbb{I}(t)-(\rho+\sigma)\mathbb{Q}(t)\right\}, \\ \mathbb{R}(t)-\mathbb{R}(0) = {}^{C}\mathbb{D}^{\delta}_{0,t}\mathbb{R}(t)\left\{\eta\mathbb{S}(t)+\sigma\mathbb{Q}(t)+\lambda\mathbb{I}(t)-\rho\mathbb{R}(t)\right\}. \end{cases} \tag{4.1}$$

After calculation

$$\begin{aligned} \mathbb{S}(t)-\mathbb{S}(0) &= \mathcal{H}(\delta)\int_0^t(t-\vartheta)^{-\delta}\mathcal{B}_1(\delta,\vartheta,\mathbb{S}(\vartheta))d\vartheta, \\ \mathbb{E}(t)-\mathbb{E}(0) &= \mathcal{H}(\delta)\int_0^t(t-\vartheta)^{-\delta}\mathcal{B}_2(\delta,\vartheta,\mathbb{E}(\vartheta))d\vartheta, \\ \mathbb{I}(t)-\mathbb{I}(0) &= \mathcal{H}(\delta)\int_0^t(t-\vartheta)^{-\delta}\mathcal{B}_4\left(\delta,\vartheta,\mathbb{I}(\vartheta)\right)d\vartheta, \\ \mathbb{Q}(t)-\mathbb{Q}(0) &= \mathcal{H}(\delta)\int_0^t(t-\vartheta)^{-\delta}\mathcal{B}_3\left(\delta,\vartheta,\mathbb{Q}(\vartheta)\right)d\vartheta, \\ \mathbb{R}(t)-\mathbb{R}(0) &= \mathcal{H}(\delta)\int_0^t(t-\vartheta)^{-\delta}\mathcal{B}_5(\delta,\vartheta,\mathbb{R}(\vartheta))d\vartheta, \end{aligned} \tag{4.2}$$

where

$$\begin{cases} \mathbb{S}(t)-\mathbb{S}(0) = {}^{C}\mathbb{D}^{\delta}_{0,t}\mathbb{S}(t)\left\{B-\theta\mathbb{S}\mathbb{I}(1+\tau\mathbb{I})-(\varepsilon_1+\rho+\eta)\mathbb{S}(t)\right\}, \\ \mathbb{E}(t)-\mathbb{E}(0) = {}^{C}\mathbb{D}^{\delta}_{0,t}\mathbb{E}(t)\left\{\theta\mathbb{S}\mathbb{I}(1+\tau\mathbb{I})-(\varepsilon_2+\rho+\varphi)\mathbb{E}(t)\right\}, \\ \mathbb{I}(t)-\mathbb{I}(0) = {}^{C}\mathbb{D}^{\delta}_{0,t}\mathbb{I}(t)\left\{\varphi\mathbb{E}(t)-(\lambda+\epsilon+\rho+\varepsilon_3)\mathbb{I}(t)\right\}, \\ \mathbb{Q}(t)-\mathbb{Q}(0) = {}^{C}\mathbb{D}^{\delta}_{0,t}\mathbb{Q}(t)\left\{\varepsilon_1\mathbb{S}(t)+\varepsilon_2\mathbb{E}(t)+\varepsilon_3\mathbb{I}(t)-(\rho+\sigma)\mathbb{Q}(t)\right\}, \\ \mathbb{R}(t)-\mathbb{R}(0) = {}^{C}\mathbb{D}^{\delta}_{0,t}\mathbb{R}(t)\left\{\eta\mathbb{S}(t)+\sigma\mathbb{Q}(t)+\lambda\mathbb{I}(t)-\rho\mathbb{R}(t)\right\}. \end{cases} \tag{4.3}$$

$$\begin{aligned} \mathcal{B}_1(\delta,t,\mathbb{S}(t)) &= B-\theta\mathbb{S}\mathbb{I}(1+\tau\mathbb{I})-(\varepsilon_1+\rho+\eta)\mathbb{S}(t), \\ \mathcal{B}_2(\delta,t,\mathbb{E}(t)) &= \theta\mathbb{S}\mathbb{I}(1+\tau\mathbb{I})-(\varepsilon_2+\rho+\varphi)\mathbb{E}(t), \\ \mathcal{B}_3\left(\delta,t,\mathbb{I}(t)\right) &= \varphi\mathbb{E}(t)-(\lambda+\epsilon+\rho+\varepsilon_3)\mathbb{I}(t), \\ \mathcal{B}_4\left(\delta,t,\mathbb{Q}(t)\right) &= \varepsilon_1\mathbb{S}(t)+\varepsilon_2\mathbb{E}(t)+\varepsilon_3\mathbb{I}(t)-(\rho+\sigma)\mathbb{Q}(t), \\ \mathcal{B}_5(\delta,t,\mathbb{R}(t)) &= \eta\mathbb{S}(t)+\sigma\mathbb{Q}(t)+\lambda\mathbb{I}(t)-\rho\mathbb{R}(t). \end{aligned} \tag{4.4}$$

The symbols $\mathcal{B}_1$,$\mathcal{B}_2$,$\mathcal{B}_3$,$\mathcal{B}_4$ and $\mathcal{B}_5$ have to hold for the Lipschitz condition only if $\mathbb{S}(t), \mathbb{E}(t), \mathbb{Q}(t), \mathbb{I}(t)$ and $\mathbb{R}(t)$ possess an upper bound. Summarizing that $\mathbb{S}(t)$ and $\mathbb{S}^*(t)$ are couple functions, we reach

$$\left\|\mathcal{B}_1(\delta,t,\mathbb{S}(t))-\mathcal{B}_1\left(\delta,t,\mathbb{S}^*(t)\right)\right\| = \left\|-\left(\theta\mathbb{I}(1+\tau\mathbb{I})+\eta+\rho+\varepsilon_1\right)\left(\mathbb{S}(t)-\mathbb{S}^*(t)\right)\right\|. \tag{4.5}$$

Taking into account $\Lambda_1 = \left\|-\left(\theta\mathbb{I}(1+\tau\mathbb{I})+\eta+\rho+\varepsilon_1\right)\right\|$ one reaches

$$\left\|\mathcal{B}_1(\delta,t,\mathbb{S}(t))-\mathcal{B}_1\left(\delta,t,\mathbb{S}^*(t)\right)\right\| \leq \Lambda_1\left\|\mathbb{S}(t)-\mathbb{S}^*(t)\right\|. \tag{4.6}$$

Similarly

$$\begin{aligned}
&\|\mathcal{B}_2(\delta,t,\mathbb{E}(t))-\mathcal{B}_2(\delta,t,\mathbb{E}^*(t))\|\leq\Lambda_2\|\mathbb{E}(t)-\mathbb{E}^*(t)\|,\\
&\|\mathcal{B}_3(\delta,t,\mathbb{Q}(t))-\mathcal{B}_3(\delta,t,\mathbb{Q}^*(t))\|\leq\Lambda_3\|\mathbb{Q}(t)-\mathbb{Q}^*(t)\|,\\
&\|\mathcal{B}_4(\delta,t,\mathbb{I}(t))-\mathcal{B}_4(\delta,t,\mathbb{I}^*(t))\|\leq\Lambda_4\|\mathbb{I}(t)-\mathbb{I}^*(t)\|,\\
&\|\mathcal{B}_5(\delta,t,\mathbb{R}(t))-\mathcal{B}_5(\delta,t,\mathbb{R}^*(t))\|\leq\Lambda_5\|\mathbb{R}(t)-\mathbb{R}^*(t)\|.
\end{aligned}\tag{4.7}$$

Where

$$\begin{aligned}
\Lambda_2&=\|-(\varphi+\rho+\varepsilon_2)\|\\
\Lambda_3&=\|-(\rho+\epsilon+\lambda+\varepsilon_3)\|\\
\Lambda_4&=\|-(\rho+\tau)\|\\
\Lambda_5&=\|-(\rho)\|.
\end{aligned}$$

These results suggest that the Lipschitz condition holds for all five functions. By iteratively utilizing the equations in (4.2), we can derive the following expressions

$$\begin{aligned}
\mathbb{S}_n(t)&=\mathcal{H}(\delta)\int_0^t(t-\vartheta)^{-\delta}\mathcal{B}_1(\delta,\vartheta,\mathbb{S}_{n-1}(\vartheta))\,d\vartheta,\\
\mathbb{E}_n(t)&=\mathcal{H}(\delta)\int_0^t(t-\vartheta)^{-\delta}\mathcal{B}_2(\delta,\vartheta,\mathbb{E}_{n-1}(\vartheta))\,d\vartheta,\\
\mathbb{Q}_n(t)&=\mathcal{H}(\delta)\int_0^t(t-\vartheta)^{-\delta}\mathcal{B}_3(\delta,\vartheta,\mathbb{Q}_{n-1}(\vartheta))\,d\vartheta,\\
\mathbb{I}_n(t)&=\mathcal{H}(\delta)\int_0^t(t-\vartheta)^{-\delta}\mathcal{B}_4(\delta,\vartheta,\mathbb{I}_{n-1}(\vartheta))\,d\vartheta,\\
\mathbb{R}_n(t)&=\mathcal{H}(\delta)\int_0^t(t-\vartheta)^{-\delta}\mathcal{B}_5(\delta,\vartheta,\mathbb{R}_{n-1}(\vartheta))\,d\vartheta,
\end{aligned}\tag{4.8}$$

together with $\mathbb{S}_0(t)=\mathbb{S}(0),\mathbb{E}_0(t)=\mathbb{E}(0),\mathbb{Q}_0(t)=\mathbb{Q}(0),\mathbb{I}_0(t)=\mathbb{I}(0)$ and $\mathbb{R}_0(t)=\mathbb{R}(0)$. When the successive terms difference is taken, we get

$$
\begin{aligned}
\Psi_{\mathbb{S},n}(t) =& \mathbb{S}_n(t) - \mathbb{S}_{n-1}(t) \\
=& \mathcal{H}(\delta) \int_0^t (t-\vartheta)^{-\delta} \left(\mathcal{B}_1\left(\delta, \vartheta, \mathbb{S}_{n-1}(\vartheta)\right) - \mathcal{B}_1\left(\delta, \vartheta, \mathbb{S}_{n-2}(\vartheta)\right)\right) d\vartheta, \\
\Psi_{\mathbb{E},n}(t) =& \mathbb{E}_n(t) - \mathbb{E}_{n-1}(t) \\
=& \mathcal{H}(\delta) \int_0^l (t-\vartheta)^{-\delta} \left(\mathcal{B}_2\left(\delta, \vartheta, \mathbb{E}_{n-1}(\vartheta)\right) - \mathcal{B}_2\left(\delta, \vartheta, \mathbb{E}_{n-2}(\vartheta)\right)\right) d\vartheta, \\
\Psi_{\mathbb{I},n}(t) =& \mathbb{I}_{2n}(t) - \mathbb{I}_{n-1}(t) \\
=& \mathcal{H}(\delta) \int_0^t (t-\vartheta)^{-\delta} \left(\mathcal{B}_4\left(\delta, \vartheta, \mathbb{I}_{n-1}(\vartheta)\right) - \mathcal{B}_4\left(\delta, \vartheta, \mathbb{I}_{n-2}(\vartheta)\right)\right) d\vartheta, \\
\Psi_{\mathbb{Q},n}(t) =& \mathbb{Q}_{1n}(t) - \mathbb{Q}_{n-1}(t) \\
=& \mathcal{H}(\delta) \int_0^t (t-\vartheta)^{-\delta} \left(\mathcal{B}_3\left(\delta, \vartheta, \mathbb{Q}_{n-1}(\vartheta)\right) - \mathcal{B}_3\left(\delta, \vartheta, \mathbb{Q}_{n-2}(\vartheta)\right)\right) d\vartheta, \\
\Psi_{\mathbb{R},n}(t) =& \mathbb{R}_n(t) - \mathbb{R}_{n-1}(t) \\
=& \mathcal{H}(\delta) \int_0^t (t-\vartheta)^{-\delta} \left(\mathcal{B}_5\left(\delta, \vartheta, \mathbb{R}_{n-1}(\vartheta)\right) - \mathcal{B}_5\left(\delta, \vartheta, \mathbb{R}_{n-2}(\vartheta)\right)\right) d\vartheta.
\end{aligned} \tag{4.9}
$$

It is vital to observe that

$$
\mathbb{S}_n(t) = \sum_{m=0}^{n} \Psi_{\mathbb{S},m}(t), \quad \mathbb{E}_n(t) = \sum_{m=0}^{n} \Psi_{\mathbb{E},m}(t), \quad \mathbb{Q}_n(t) = \sum_{m=0}^{n} \Psi_{\mathbb{Q},m}(t),
$$
$$
\mathbb{I}_n(t) = \sum_{m=0}^{n} \Psi_{\mathbb{I},m}(t), \quad \mathbb{R}_n(t) = \sum_{m=0}^{n} \Psi_{\mathbb{R},m}(t).
$$

Additionally, by using Eqs (4.6) and (4.7) and considering that

$$
\Psi_{\mathbb{S},n-1}(t) = \mathbb{S}_{n-1}(t) - \mathbb{S}_{n-2}(t), \quad \Psi_{\mathbb{E},n-1}(t) = \mathbb{E}_{n-1}(t) - \mathbb{E}_{n-2}(t), \quad \Psi_{\mathbb{Q},n-1}(t) = \mathbb{Q}_{n-1}(t) - \mathbb{Q}_{n-2}(t),
$$
$$
\Psi_{\mathbb{I},n-1}(t) = \mathbb{I}_{n-1}(t) - \mathbb{I}_{n-2}(t), \quad \Psi_{\mathbb{R},n-1}(t) = \mathbb{R}_{n-1}(t) - \mathbb{R}_{n-2}(t),
$$

we reach

$$
\begin{aligned}
&\left\|\Psi_{\mathbb{S},n}(t)\right\| \leq \mathcal{H}(\delta)\Lambda_1 \int_0^t (t-\vartheta)^{-\delta} \left\|\Psi_{\mathbb{S},n-1}(\vartheta)\right\| d\vartheta, \\
&\left\|\Psi_{\mathbb{E},n}(t)\right\| \leq \mathcal{H}(\delta)\Lambda_2 \int_0^t (t-\vartheta)^{-\delta} \left\|\Psi_{\mathbb{E},n-1}(\vartheta)\right\| d\vartheta, \\
&\left\|\Psi_{\mathbb{I},n}(t)\right\| \leq \mathcal{H}(\delta)\Lambda_4 \int_0^t (t-\vartheta)^{-\delta} \left\|\Psi_{\mathbb{I},n-1}(\vartheta)\right\| d\vartheta, \\
&\left\|\Psi_{\mathbb{Q},n}(t)\right\| \leq \mathcal{H}(\delta)\Lambda_3 \int_0^t (t-\vartheta)^{-\delta} \left\|\Psi_{\mathbb{Q},n-1}(\vartheta)\right\| d\vartheta, \\
&\left\|\Psi_{\mathbb{R},n}(t)\right\| \leq \mathcal{H}(\delta)\Lambda_5 \int_0^t (t-\vartheta)^{-\delta} \left\|\Psi_{\mathbb{R},n-1}(\vartheta)\right\| d\vartheta.
\end{aligned} \tag{4.10}
$$

Theorem 3. *If the following condition holds*

$$
\frac{\mathcal{H}(\delta)}{\delta} \kappa^{\delta} \Lambda_m < 1, m = 1, 2, \ldots, 5. \tag{4.11}
$$

Then, (3.4) has a unique solution for $t \in [0, \kappa]$.

Proof It is shown that $\mathbb{S}(t), \mathbb{E}(t), \mathbb{Q}(t), \mathbb{I}(t)$ and $\mathbb{R}(t)$ are bounded functions. In addition, as can be seen from Eqs (4.6) and (4.7), the $\mathcal{B}_1$,$\mathcal{B}_2$,$\mathcal{B}_3$,$\mathcal{B}_4$ and $\mathcal{B}_5$ hold for Lipchitz condition. Therefore, utilizing Eq (4.10) together with a recursive hypothesis, we arrive at

$$\begin{aligned}
\left\|\Psi_{\mathbb{S},n}(t)\right\| &\leq \|\mathbb{S}_0(t)\| \left(\tfrac{\mathcal{H}(\delta)}{\delta}\kappa^{\delta}\Lambda_1\right)^n, \\
\left\|\Psi_{\mathbb{E},n}(t)\right\| &\leq \|\mathbb{E}_0(t)\| \left(\tfrac{\mathcal{H}(\delta)}{\delta}\kappa^{\delta}\Lambda_2\right)^n, \\
\left\|\Psi_{\mathbb{I},n}(t)\right\| &\leq \|\mathbb{I}_0(t)\| \left(\tfrac{\mathcal{H}(\delta)}{\delta}\kappa^{\delta}\Lambda_4\right)^n, \\
\left\|\Psi_{\mathbb{Q},n}(t)\right\| &\leq \|\mathbb{Q}_0(t)\| \left(\tfrac{\mathcal{H}(\delta)}{\delta}\kappa^{\delta}\Lambda_3\right)^n, \\
\left\|\Psi_{\mathbb{R},n}(t)\right\| &\leq \|\mathbb{R}_0(t)\| \left(\tfrac{\mathcal{H}(\delta)}{\delta}\kappa^{\delta}\Lambda_5\right)^n.
\end{aligned} \tag{4.12}$$

As a result, it is evident that sequences fulfill and exist

$$\left\|\Psi_{\mathbb{S},n}(t)\right\| \to 0, \left\|\Psi_{\mathbb{E},n}(t)\right\| \to 0, \left\|\Psi_{\mathbb{I},n}(t)\right\| \to 0, \left\|\Psi_{\mathbb{Q},n}(t)\right\| \to 0, \quad \left\|\Psi_{\mathbb{R},n}(t)\right\| \to 0 \text{ as } n \to \infty.$$

Additionally, using Eq (4.12) and the triangle inequality, for any s, we have

$$\begin{aligned}
\|\mathbb{S}_{n+s}(t) - \mathbb{S}_n(t)\| &\leq \textstyle\sum_{j=n+1}^{n+s} X_1^j = \frac{X_1^{n+1} - X_1^{n+s+1}}{1-X_1}, \\
\|\mathbb{E}_{n+s}(t) - \mathbb{E}_n(t)\| &\leq \textstyle\sum_{j=n+1}^{n+s} X_2^j = \frac{X_2^{n+1} - X_2^{n+s+1}}{1-X_2}, \\
\|\mathbb{I}_{n+s}(t) - \mathbb{I}_n(t)\| &\leq \textstyle\sum_{j=n+1}^{n+s} X_3^j = \frac{X_3^{n+1} - X_3^{n+s+1}}{1-X_3}, \\
\|\mathbb{Q}_{n+s}(t) - \mathbb{Q}_n(t)\| &\leq \textstyle\sum_{j=n+1}^{n+s} X_4^j = \frac{X_4^{n+1} - X_4^{n+s+1}}{1-X_4}, \\
\|\mathbb{R}_{n+s}(t) - \mathbb{R}_n(t)\| &\leq \textstyle\sum_{m=n+1}^{n+s} X_5^j = \frac{X_5^{n+1} - X_5^{n+s+1}}{1-X_5},
\end{aligned} \tag{4.13}$$

with $X_m = \frac{\mathcal{H}(\delta)}{\delta}\kappa^{\delta}\Lambda_m < 1$ by hypothesis. Consequently, the sequences $\mathbb{S}_n$, $\mathbb{E}_n$, $\mathbb{I}_n$, $\mathbb{Q}_n$, and $\mathbb{R}_n$ can be considered as Cauchy sequences in the Banach space $\mathcal{A}(Y)$. It has been shown that they converge uniformly [49].

5. Parameter estimation

Parameter estimation is a fundamental problem in statistical inference, machine learning, and many other fields. It involves estimating the values of unknown parameters in a model based on observed data. The goal of parameter estimation is to find the values of the parameters that best fit the data and allow us to make accurate predictions or draw meaningful conclusions about the system under study. There are many different methods for parameter estimation, ranging from simple techniques like least squares regression to more complex approaches like maximum likelihood estimation or Bayesian

inference. The choice of method often depends on the nature of the data, the complexity of the model, and the specific goals of the analysis. However, regardless of the method chosen, parameter estimation is a crucial step in many scientific and engineering applications, and its success or failure can have significant consequences.

In this part, we used the least square curve fitting methods to analyze the instances of COVID-19 that were reported in India between 13 July 2021 and 25 August 2021 [50]. The system's (3.4) estimated parameters are based on India's overall data on conformed events and fatalities. The daily reports' error terms are reduced using the ordinary least square solution (OLS), and the goodness of fit test uses the related relative error.

$$\min\left(\frac{\sum_{\iota=1}^{n}\left(\mathbb{I}_{\iota}-\hat{\mathbb{I}}_{l}\right)^{2}}{\sum_{\iota=1}^{n}\mathbb{I}_{\iota}^{2}}\right). \tag{5.1}$$

Table 1. The Table contains descriptions and estimated values for the parameters.

Symbol of parameters	Values of parameters	References
B	60.5089	Fitted
θ	0.0477	Estimated
τ	0.0205	Estimated
ϵ	0.1571	Estimated
ε_1	0.0805	Estimated
ε_2	0.0176	Estimated
ε_3	0.0309	Estimated
ρ	0.3506	Fitted
η	0.1805	Estimated
α	0.0059	Estimated
σ	0.0009	Fitted
λ	0.0894	Estimated

6. Sensitivity analysis

Sensitivity analysis plays a crucial role in identifying the parameters that are most effective in controlling the spread of COVID-19. Although forward sensitivity analysis can be laborious for complex biological models, it remains an essential component of phenomena modeling. Ecologists and epidemiologists have shown considerable interest in conducting sensitivity analysis of R_0.

Definition 4. *The normalized forward sensitivity index of R_0 that depends on the differentiability of a parameter $\varkappa$ is described as follows:*

$$\Upsilon_{\varkappa}=\frac{\varkappa}{R_0}\frac{\partial R_0}{\partial \varkappa}.$$

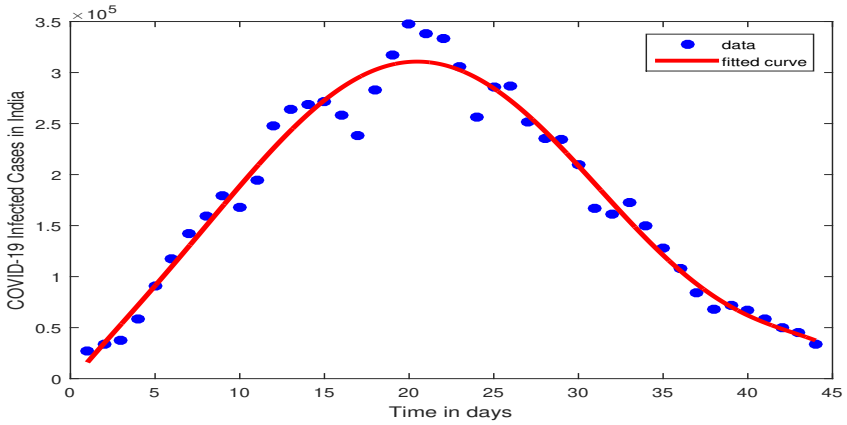

(a)

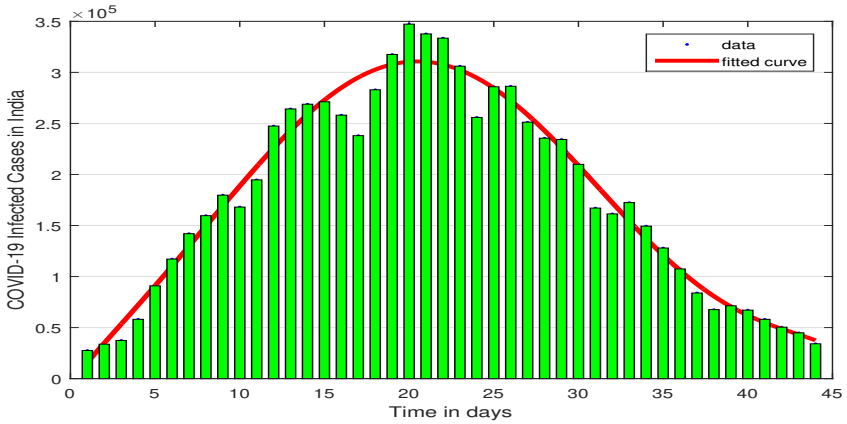

(b)

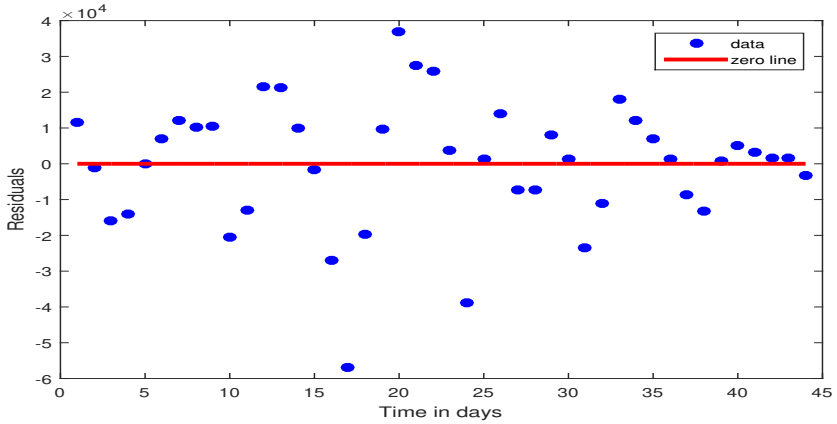

(c)

Figure 1. The simulation results for a suggested model of COVID-19 cases in India from January 1 to February 14, 2022 are shown in the figure. The best-fitted curve and its residuals, which represent the variations between the simulated results and the actual daily cumulative cases reported during that time, are displayed on the graph. The curve may serve as a decision-making tool for public health measures and interventions by assisting researchers and decision-makers in better understanding the patterns and trends of the pandemic in India.

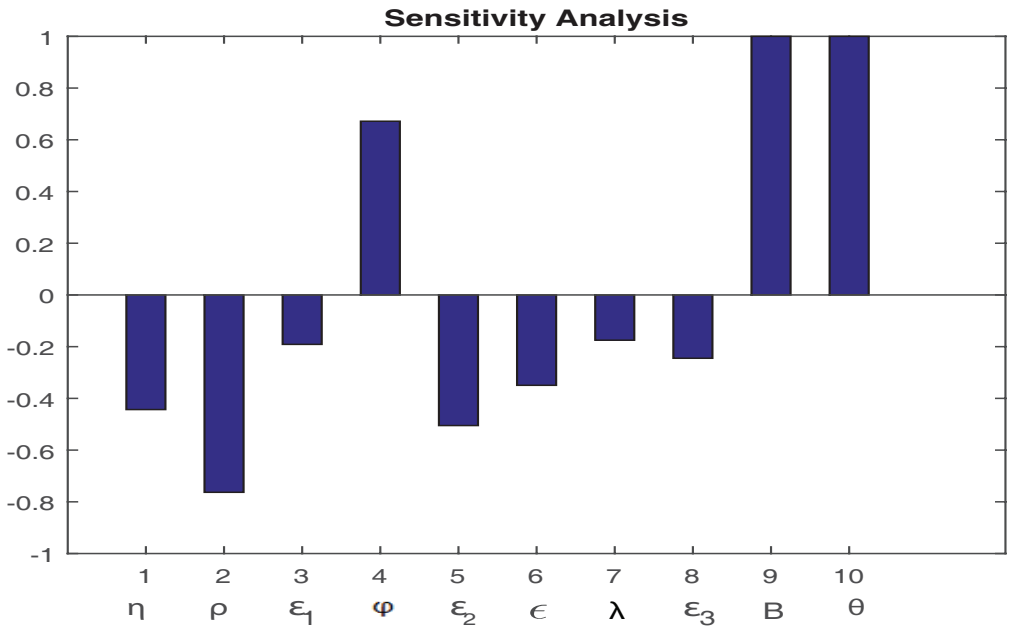

Figure 2. This plot provides a thorough evaluation of the relative significance of each input parameter by demonstrating the sensitivity of a model's output to changes in multiple input variables at once.

Sensitivity indices, which quantify the contribution of various factors to the output of a model, can be computed in a number of different ways. Direct differentiation, Latin hypercube sampling, and system linearization are three frequently used techniques. The direct differentiation method will be used in this study because it gives analytical expressions for the indices. Using this method, we can compare the variation between the R_0 parameter and other parameters and analyze the effects of various financial crime-related factors. We can learn vital information about the relative weights of various variables and how they impact the model's output by using sensitivity indices. This knowledge can enhance our comprehension of the dynamics of financial crime and assist in guiding policy decisions. The graphical results are displayed in Figures 2 and 3.

7. Numerical scheme

Consider $\dot{\mathbb{S}}(t), \dot{\mathbb{E}}(t), \dot{\mathbb{I}}(t), \dot{\mathbb{Q}}(t)$ and $\dot{\mathbb{R}}(t)$ are in the square integrable function space $L_2[0, 1)$, and can be expressed as a Haar series as

$$\dot{\mathbb{S}}(t) = \sum_{p=1}^{N} \alpha_p \tilde{\psi}_p(t), \dot{\mathbb{E}}(t) = \sum_{p=1}^{N} \theta_p \tilde{\psi}_p(t), \dot{\mathbb{I}}(t) = \sum_{p=1}^{N} \lambda_p \tilde{\psi}_p(t), \dot{\mathbb{I}}(t) = \sum_{p=1}^{N} \vartheta_p \tilde{\psi}_p(t) \text{ and } \mathbb{R}(\dot{t}) = \sum_{p=1}^{N} \sigma_p \tilde{\psi}_p(t)$$

where α_p, θ_p, λ_p, ϑ_p and σ_p are coefficients of the Haar series and $\tilde{\psi}_p(t)$ is the discretise Haar function [51] with the exposed compartment $\mathbb{E}_0$ includes people who have been infected but are not yet contagious, and the susceptible compartment $\mathbb{S}_0$ represents people who are initially susceptible to the disease at the start of the epidemic. The infectious individuals are housed in the infected compartment

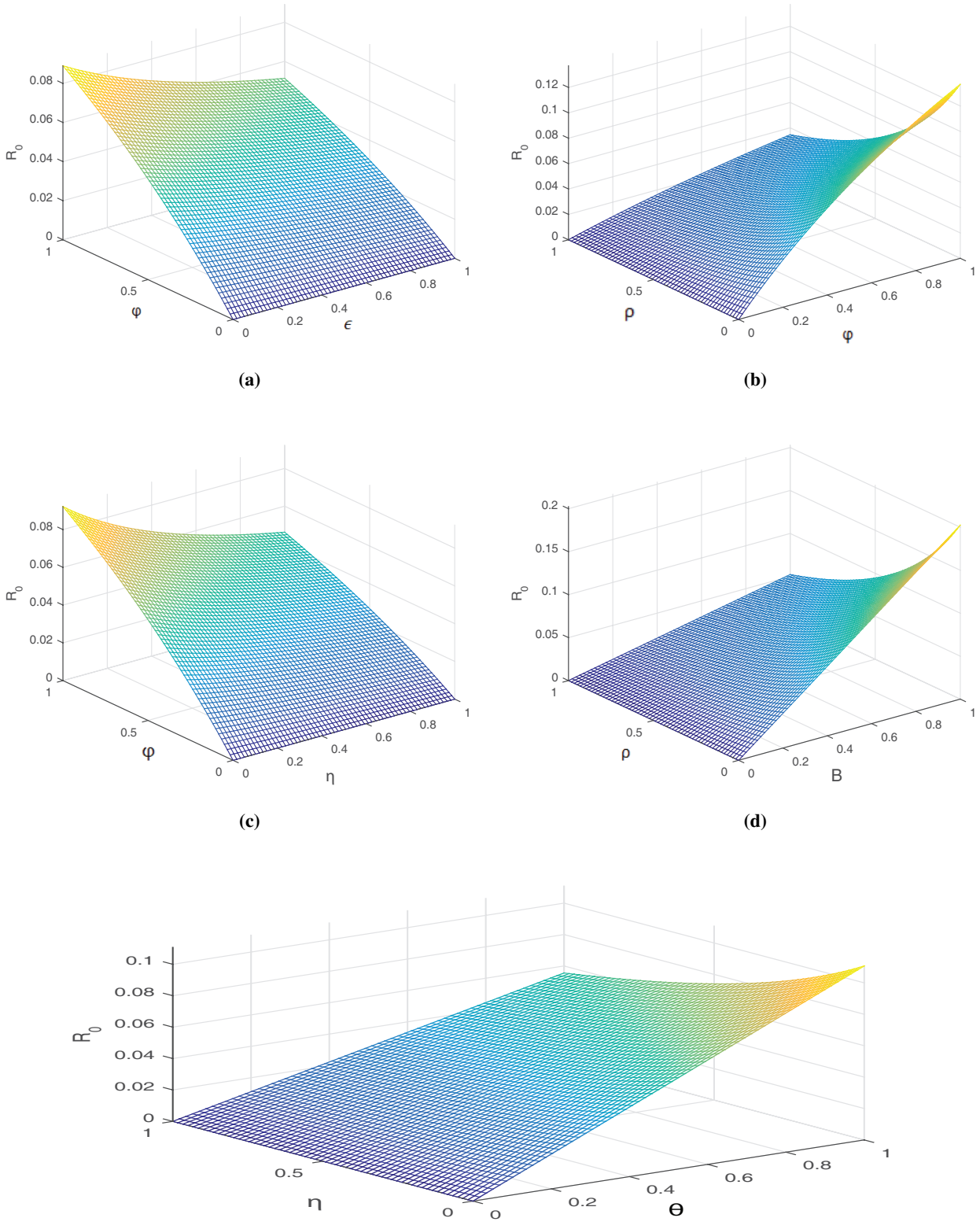

Figure 3. The plot represents the sensitivity of various parameters against R_0.

$\mathbb{I}_0$, whereas the isolated or hospitalized individuals are housed in the quarantined compartment $\mathbb{Q}_0$. Those who have recovered from the illness and are no longer contagious are included in the recovered compartment $\mathbb{R}_0$. We integrate the equations that describe the movement of people between these compartments in order to model the epidemic's progression over time. The result of this integration is a set of equations that show how the population of each compartment varies over time.

$$\begin{aligned}&\mathbb{S}(t) = \mathbb{S}_0 + \sum_{p=1}^{N} \alpha_p \mathcal{G}_{p,1}(t), \mathbb{E}(t) = \mathbb{E}_0 + \sum_{p=1}^{N} \theta_p \mathcal{G}_{p,1}(t), \mathbb{I}(t) = \mathbb{I}_0 + \sum_{p=1}^{N} \lambda_p \mathcal{G}_{p,1}(t),\\ &\mathbb{Q}(t) = \mathbb{Q}_0 + \sum_{p=1}^{N} \vartheta_p \mathcal{G}_{p,1}(t), \quad \text{and} \quad \mathbb{R}(t) = \mathbb{R}_0 + \sum_{p=1}^{N} \sigma_p \mathcal{G}_{p,1}(t)\end{aligned} \tag{7.1}$$

where $\mathcal{G}_{p,1}(t)$ is the operational matrix of integration of p^{th} order [51, 52].

By using Caputo derivative, we have

$$\begin{cases}\frac{1}{\Gamma(n-\delta)} \int_0^t \mathbb{S}^{(n)}(\vartheta)(t-\vartheta)^{n-\delta-1} d\vartheta = B - \theta \mathbb{S}\mathbb{I}(1+\tau\mathbb{I}) - (\varepsilon_1 + \rho + \eta)\mathbb{S}(t),\\ \frac{1}{\Gamma(n-\delta)} \int_0^t \mathbb{E}^{(n)}(\vartheta)(t-\vartheta)^{n-\delta-1} d\vartheta = \theta \mathbb{S}\mathbb{I}(1+\tau\mathbb{I}) - (\varepsilon_2 + \rho + \varphi)\mathbb{E}(t),\\ \frac{1}{\Gamma(n-\delta)} \int_0^t \mathbb{I}^{(n)}(\vartheta)(t-\vartheta)^{n-\delta-1} d\vartheta = \varphi \mathbb{E}(t) - (\lambda + \epsilon + \rho + \varepsilon_3)\mathbb{I}(t),\\ \frac{1}{\Gamma(n-\delta)} \int_0^t \mathbb{Q}^{(n)}(\vartheta)(t-\vartheta)^{n-\delta-1} d\vartheta = \varepsilon_1 \mathbb{S}(t) + \varepsilon_2 \mathbb{E}(t) + \varepsilon_3 \mathbb{I}(t) + -(\rho + \sigma)\mathbb{Q}(t),\\ \frac{1}{\Gamma(n-\delta)} \int_0^t \mathbb{R}^{(n)}(\vartheta)(t-\vartheta)^{n-\delta-1} d\vartheta = \eta \mathbb{S}(t) + \sigma \mathbb{Q}(t) + \lambda \mathbb{I}(t) - \rho \mathbb{R}(t).\end{cases} \tag{7.2}$$

As we have assumed that $0 < \delta < 1$, therefore $n = 1$, and we have

$$\begin{cases}\frac{1}{\Gamma(1-\delta)} \int_0^t \dot{\mathbb{S}}(\vartheta)(t-\vartheta)^{-\delta} d\vartheta = B - \theta \mathbb{S}\mathbb{I}(1+\tau\mathbb{I}) - (\varepsilon_1 + \rho + \eta)\mathbb{S}(t),\\ \frac{1}{\Gamma(1-\delta)} \int_0^t \dot{\mathbb{E}}(\vartheta)(t-\vartheta)^{-\delta} d\vartheta = \theta \mathbb{S}\mathbb{I}(1+\tau\mathbb{I}) - (\varepsilon_2 + \rho + \varphi)\mathbb{E}(t),\\ \frac{1}{\Gamma(1-\delta)} \int_0^t \dot{\mathbb{I}}(\vartheta)(t-\vartheta)^{-\delta} d\vartheta = \varphi \mathbb{E}(t) - (\lambda + \epsilon + \rho + \varepsilon_3)\mathbb{I}(t),\\ \frac{1}{\Gamma(1-\delta)} \int_0^t \dot{\mathbb{Q}}(\vartheta)(t-\vartheta)^{-\delta} d\vartheta = \varepsilon_1 \mathbb{S}(t) + \varepsilon_2 \mathbb{E}(t) + \varepsilon_3 \mathbb{I}(t) - (\rho + \sigma)\mathbb{Q}(t),\\ \frac{1}{\Gamma(1-\delta)} \int_0^t \dot{\mathbb{R}}(\vartheta)(t-\vartheta)^{-\delta} d\vartheta = \eta \mathbb{S}(t) + \sigma \mathbb{Q}(t) + \lambda \mathbb{I}(t) - \rho \mathbb{R}(t).\end{cases} \tag{7.3}$$

Haar approximations are used, and we have

$$\begin{aligned}\frac{1}{\Gamma(1-\delta)} \int_0^t \sum_{p=1}^{N} \alpha_p \tilde{\psi}_p(\vartheta)(t-\vartheta)^{-\delta} d\vartheta = B - \theta \left(\mathbb{I}_0 + \sum_{p=1}^{N} \lambda_p \mathcal{G}_{p,1}(t)\right)\left(\mathbb{S}_0 + \sum_{p=1}^{N} \alpha_p \mathcal{G}_{p,1}(t)\right)\\ \left(1 + \tau\left(\mathbb{I}_0 + \sum_{p=1}^{N} \lambda_p \mathcal{G}_{p,1}(t)\right)\right) - (\varepsilon_1 + \rho + \eta)\left(\mathbb{S}_0 + \sum_{p=1}^{N} \alpha_p \mathcal{G}_{p,1}(t)\right)\end{aligned} \tag{7.4}$$

$$\frac{1}{\Gamma(1-\delta)}\int_0^t \sum_{p=1}^{N} \theta_p \tilde{\psi}_p(\vartheta)(t-\vartheta)^{-\delta}d\vartheta = \theta\left(\mathbb{I}_0 + \sum_{p=1}^{N}\lambda_p \mathcal{G}_{p,1}(t)\right)\left(\mathbb{S}_0 + \sum_{p=1}^{N}\alpha_p \mathcal{G}_{p,1}(t)\right) \left(1+\tau\left(\mathbb{I}_0 + \sum_{p=1}^{N}\lambda_p \mathcal{G}_{p,1}(t)\right)\right) - (\varepsilon_2+\rho+\varphi)\left(\mathbb{E}_0 + \sum_{p=1}^{N}\theta_p \mathcal{G}_{p,1}(t)\right) \tag{7.5}$$

$$\frac{1}{\Gamma(1-\delta)}\int_0^t \sum_{p=1}^{N} \lambda_p \tilde{\psi}_p(\vartheta)(t-\vartheta)^{-\delta}d\vartheta = \varphi\left(\mathbb{E}_0 + \sum_{p=1}^{N}\theta_p \vartheta_{p,1}(t)\right) - (\lambda+\epsilon+\rho+d_1)\left(\mathbb{I}_0 + \sum_{p=1}^{N}\lambda_p \mathcal{G}_{p,1}(t)\right) \tag{7.6}$$

$$\frac{1}{\Gamma(1-\delta)}\int_0^t \sum_{p=1}^{N} \vartheta_p \tilde{\psi}_p(\vartheta)(t-\vartheta)^{-\delta}d\vartheta = \varepsilon_3\left(\mathbb{I}_0 + \sum_{p=1}^{N}\lambda_p \mathcal{G}_{p,1}(t)\right) + \varepsilon_2\left(\mathbb{E}_0 + \sum_{p=1}^{N}\theta_p \mathcal{G}_{p,1}(t)\right) + \varepsilon_1\left(\mathbb{S}_0 + \sum_{p=1}^{N}\alpha_p \mathcal{G}_{p,1}(t)\right) - (\rho+\sigma)\left(\mathbb{Q}_0 + \sum_{p=1}^{N}\vartheta_p \mathcal{G}_{p,1}(t)\right) \tag{7.7}$$

$$\frac{1}{\Gamma(1-\delta)}\int_0^t \sum_{p=1}^{N} \alpha_p \tilde{\psi}_p(\vartheta)(t-\vartheta)^{-\delta}d\vartheta = \eta\left(\mathbb{S}_0 + \sum_{p=1}^{N}\alpha_p \mathcal{G}_{p,1}(t)\right) + \sigma\left(\mathbb{Q}_0 + \sum_{p=1}^{N}\sigma_p \vartheta_{p,1}(t)\right) + \lambda\left(\mathbb{I}_0 + \sum_{p=1}^{N}\lambda_p \mathcal{G}_{p,1}(t)\right) + \rho\left(\mathbb{R}_0 + \sum_{p=1}^{N}\zeta_p \mathcal{G}_{p,1}(t)\right) \tag{7.8}$$

Upon simplification, we have

$$\left\{\begin{array}{l} \frac{1}{\Gamma(1-\delta)}\sum_{p=1}^{N}\alpha_p\tilde{\psi}_p(\vartheta)(t-\vartheta)^{-\delta}d\vartheta - B + \theta(1+\tau\mathbb{I}_0)\times \\ \left(\mathbb{I}_0\mathbb{S}_0 + \mathbb{I}_0\sum_{p=1}^{N}\alpha_p\mathcal{G}_{p,1}(t) + \mathbb{S}_0\sum_{p=1}^{N}\theta_p\mathcal{G}_{p,1}(t) + \sum_{p=1}^{N}\alpha_p\mathcal{G}_{p,1}(t)\sum_{p=1}^{N}\theta_p\mathcal{G}_{p,1}(t)\right) \\ +\theta\left[\mathbb{I}_0\mathbb{S}_0\tau\sum_{p=1}^{N}\theta_p\mathcal{G}_{p,1}(t) + \mathbb{I}_0\tau\sum_{p=1}^{N}\alpha_p\mathcal{G}_{p,1}(t)\sum_{p=1}^{N}\theta_p\mathcal{G}_{p,1}(t) + \mathbb{S}_0\tau\left(\sum_{p=1}^{N}\theta_p\mathcal{G}_{p,1}(t)\right)^2\right. \\ \left. +\tau\sum_{p=1}^{N}\alpha_p\mathcal{G}_{p,1}(t)\left(\sum_{p=1}^{N}\theta_p\mathcal{G}_{p,1}(t)\right)^2\right] + (\varepsilon_1+\rho+\eta)\mathbb{S}_0 + (\varepsilon_1+\rho+\eta)\sum_{p=1}^{N}\alpha_p\mathcal{G}_{p,1}(t) \end{array}\right\} = 0, \tag{7.9}$$

$$\left\{\begin{array}{l} \frac{1}{\Gamma(1-\delta)}\sum_{p=1}^{N}\theta_p\tilde{\psi}_p(\vartheta)(t-\vartheta)^{-\delta}d\vartheta + \theta(1+\tau\mathbb{I}_0)\times \\ \left(\mathbb{I}_0\mathbb{S}_0 + \mathbb{I}_0\sum_{p=1}^{N}\alpha_p\mathcal{G}_{p,1}(t) + \mathbb{S}_0\sum_{p=1}^{N}\theta_p\mathcal{G}_{p,1}(t) + \sum_{p=1}^{N}\alpha_p\mathcal{G}_{p,1}(t)\sum_{p=1}^{N}\theta_p\mathcal{G}_{p,1}(t)\right) \\ +\theta\left[\mathbb{I}_0\mathbb{S}_0\tau\sum_{p=1}^{N}\theta_p\mathcal{G}_{p,1}(t) + \mathbb{I}_0\tau\sum_{p=1}^{N}\alpha_p\mathcal{G}_{p,1}(t)\sum_{p=1}^{N}\theta_p\mathcal{G}_{p,1}(t) + \mathbb{S}_0\tau\left(\sum_{p=1}^{N}\theta_p\mathcal{G}_{p,1}(t)\right)^2\right. \\ \left. +\tau\sum_{p=1}^{N}\alpha_p\mathcal{G}_{p,1}(t)\left(\sum_{p=1}^{N}\theta_p\mathcal{G}_{p,1}(t)\right)^2\right] + (\varepsilon_2+\rho+\varphi)\mathbb{E}_0 + (\varepsilon_2+\rho+\varphi)\sum_{p=1}^{N}\theta_p\mathcal{G}_{p,1}(t) \end{array}\right\} = 0, \tag{7.10}$$

$$\frac{1}{\Gamma(1-\delta)}\int_0^t \sum_{p=1}^{N} \lambda_p \tilde{\psi}_p(\vartheta)(t-\vartheta)^{-\delta} d\vartheta - \varphi\mathbb{E}_0 - \varphi\left(\sum_{p=1}^{N} \theta_p \mathcal{G}_{p,1}(t)\right) + (\lambda+\epsilon+\rho+\varepsilon_3)\mathbb{I}_0 + (\lambda+\epsilon+\rho+\varepsilon_3)\left(\sum_{p=1}^{N} \lambda_p \mathcal{G}_{p,1}(t)\right) = 0, \tag{7.11}$$

$$\frac{1}{\Gamma(1-\delta)}\int_0^t \sum_{p=1}^{N} \vartheta_p \tilde{\psi}_p(\vartheta)(t-\vartheta)^{-\delta} d\vartheta - \varepsilon_3\mathbb{I}_0 - \varepsilon_3\left(\sum_{p=1}^{N} \lambda_p \mathcal{G}_{p,1}(t)\right) + \varepsilon_2\mathbb{E}_0 + \varepsilon_2\left(\sum_{p=1}^{N} \theta_p \mathcal{G}_{p,1}(t)\right) + \varepsilon_1\mathbb{S}_0 + \varepsilon_1\left(\sum_{p=1}^{N} \alpha_p \mathcal{G}_{p,1}(t)\right) + (\rho+\sigma)\mathbb{Q}_0 + (\rho+\sigma)\left(\sum_{p=1}^{N} \vartheta_p \vartheta_{p,1}(t)\right) = 0, \tag{7.12}$$

$$\frac{1}{\Gamma(1-\delta)}\int_0^t \sum_{p=1}^{N} \zeta_p \tilde{\psi}_p(\vartheta)(t-\vartheta)^{-\delta} d\vartheta - \eta\mathbb{S}_0 - \mathbb{S}_0\left(\sum_{p=1}^{N} \alpha_p \mathcal{G}_{p,1}(t)\right) - \sigma\mathbb{Q}_0 - \sigma\left(\sum_{p=1}^{N} \sigma_p \mathcal{G}_{p,1}(t)\right) - \lambda\mathbb{I}_0 - \lambda\left(\sum_{p=1}^{N} \lambda_p \mathcal{G}_{p,1}(t)\right) + \rho\mathbb{R}_0 + \rho\left(\sum_{p=1}^{N} \zeta_p \mathcal{G}_{p,1}(t)\right) = 0. \tag{7.13}$$

Applying the Haar integration method [53], we can estimate the integral in the aforementioned system as an approximation, given by:

$$\int_{\varkappa}^{\kappa} f(t)dt \approx \frac{\kappa-\varkappa}{N}\sum_{p=1}^{N} f\left(t_p\right) = \sum_{p=1}^{N} f\left(\varkappa + \frac{(\kappa-\varkappa)(p-0.5)}{N}\right) \tag{7.14}$$

$$\left\{\begin{array}{l} \frac{t}{N\Gamma(1-\delta)}\sum_{s=1}^{N}\sum_{p=1}^{N} \alpha_p \tilde{\psi}_p\left(\vartheta_s\right)\left(t-\vartheta_s\right)^{-\delta} - B + \theta\left(1+\tau\mathbb{I}_0\right)\times \\ \left(\mathbb{I}_0\mathbb{S}_0 + \mathbb{I}_0\sum_{p=1}^{N} \alpha_p \mathcal{G}_{p,1}(t) + \mathbb{S}_0\sum_{p=1}^{N} \theta_p \mathcal{G}_{p,1}(t) + \sum_{p=1}^{N} \alpha_p \mathcal{G}_{p,1}(t)\sum_{p=1}^{N} \theta_p \mathcal{G}_{p,1}(t)\right) \\ +\theta\left[\mathbb{I}_0\mathbb{S}_0\tau\sum_{p=1}^{N} \theta_p \mathcal{G}_{p,1}(t) + \mathbb{I}_0\tau\sum_{p=1}^{N} \alpha_p \mathcal{G}_{p,1}(t)\sum_{p=1}^{N} \theta_p \mathcal{G}_{p,1}(t) + \mathbb{S}_0\tau\left(\sum_{p=1}^{N} \theta_p \mathcal{G}_{p,1}(t)\right)^2\right. \\ \left. +\tau\sum_{p=1}^{N} \alpha_p \mathcal{G}_{p,1}(t)\left(\sum_{p=1}^{N} \theta_p \mathcal{G}_{p,1}(t)\right)^2\right] + (\varepsilon_1+\rho+\eta)\mathbb{S}_0 + (\varepsilon_1+\rho+\eta)\sum_{p=1}^{N} \alpha_p \mathcal{G}_{p,1}(t) \end{array}\right\} = 0 \tag{7.15}$$

$$\left\{\begin{array}{l} \frac{t}{N\Gamma(1-\delta)}\sum_{s=1}^{N}\sum_{p=1}^{N} \theta_p \tilde{\psi}_p\left(\vartheta_s\right)\left(t-\vartheta_s\right)^{-\delta} - \theta\left(1+\tau\mathbb{I}_0\right)\times \\ \left(\mathbb{I}_0\mathbb{S}_0 + \mathbb{I}_0\sum_{p=1}^{N} \alpha_p \mathcal{G}_{p,1}(t) + \mathbb{S}_0\sum_{p=1}^{N} \theta_p \mathcal{G}_{p,1}(t) + \sum_{p=1}^{N} \alpha_p \mathcal{G}_{p,1}(t)\sum_{p=1}^{N} \theta_p \mathcal{G}_{p,1}(t)\right) \\ +\theta\left[\mathbb{I}_0\mathbb{S}_0\tau\sum_{p=1}^{N} \theta_p \mathcal{G}_{p,1}(t) + \mathbb{I}_0\tau\sum_{p=1}^{N} \alpha_p \mathcal{G}_{p,1}(t)\sum_{p=1}^{N} \theta_p \mathcal{G}_{p,1}(t) + \mathbb{S}_0\tau\left(\sum_{p=1}^{N} \theta_p \mathcal{G}_{p,1}(t)\right)^2\right. \\ \left. +\tau\sum_{p=1}^{N} \alpha_p \mathcal{G}_{p,1}(t)\left(\sum_{p=1}^{N} \theta_p \mathcal{G}_{p,1}(t)\right)^2\right] + (\varepsilon_2+\rho+\varphi)\mathbb{E}_0 + (\varepsilon_2+\rho+\varphi)\sum_{p=1}^{N} \theta_p \mathcal{G}_{p,1}(t) \end{array}\right\} = 0, \tag{7.16}$$

$$\frac{t}{N\Gamma(1-\delta)}\sum_{s=1}^{N}\sum_{p=1}^{N}\lambda_p\tilde{\psi}_p(\vartheta_s)(t-\vartheta_s)^{-\delta}-\varphi\mathbb{E}_0-\varphi\left(\sum_{p=1}^{N}\theta_p\mathcal{G}_{p,1}(t)\right)$$
$$+(\lambda+\epsilon+\rho+\varepsilon_3)\mathbb{I}_0+(\lambda+\epsilon+\rho+\varepsilon_3)\left(\sum_{p=1}^{N}\lambda_p\mathcal{G}_{p,1}(t)\right)=0, \tag{7.17}$$

$$\frac{t}{N\Gamma(1-\delta)}\sum_{s=1}^{N}\sum_{p=1}^{N}\vartheta_p\tilde{\psi}_p(\vartheta_s)(t-\vartheta_s)^{-\delta}-\varepsilon_3\mathbb{I}_0-\varepsilon_3\left(\sum_{p=1}^{N}\lambda_p\mathcal{G}_{p,1}(t)\right)+\varepsilon_2\mathbb{E}_0+\varepsilon_2\left(\sum_{p=1}^{N}\theta_p\mathcal{G}_{p,1}(t)\right)$$
$$+\varepsilon_1\mathbb{S}_0+\varepsilon_1\left(\sum_{p=1}^{N}\alpha_p\mathcal{G}_{p,1}(t)\right)+(\rho+\sigma)\mathbb{Q}_0+(\rho+\sigma)\left(\sum_{p=1}^{N}\vartheta_p\vartheta_{p,1}(t)\right)=0, \tag{7.18}$$

$$\frac{t}{N\Gamma(1-\delta)}\sum_{s=1}^{N}\sum_{p=1}^{N}\zeta_p\tilde{\psi}_p(\vartheta_s)(t-\vartheta_s)^{-\delta}-\eta\mathbb{S}_0-\mathbb{S}_0\left(\sum_{p=1}^{N}\alpha_p\mathcal{G}_{p,1}(t)\right)-\sigma\mathbb{Q}_0$$
$$-\sigma\left(\sum_{p=1}^{N}\sigma_p\mathcal{G}_{p,1}(t)\right)-\lambda\mathbb{I}_0-\lambda\left(\sum_{p=1}^{N}\lambda_p\mathcal{G}_{p,1}(t)\right)+\rho\mathbb{R}_0+\rho\left(\sum_{p=1}^{N}\zeta_p\mathcal{G}_{p,1}(t)\right)=0. \tag{7.19}$$

Let

$$\Phi_{1,j}=\begin{cases}\frac{t}{N\Gamma(1-\delta)}\sum_{s=1}^{N}\sum_{p=1}^{N}\alpha_p\tilde{\psi}_p(\vartheta_s)(t-\vartheta_s)^{-\delta}-B+\theta(1+\tau\mathbb{I}_0)\times\\ \left(\mathbb{I}_0\mathbb{S}_0+\mathbb{I}_0\sum_{p=1}^{N}\alpha_p\mathcal{G}_{p,1}(t)+\mathbb{S}_0\sum_{p=1}^{N}\theta_p\mathcal{G}_{p,1}(t)+\sum_{p=1}^{N}\alpha_p\mathcal{G}_{p,1}(t)\sum_{p=1}^{N}\theta_p\mathcal{G}_{p,1}(t)\right)\\ +\theta\left[\mathbb{I}_0\mathbb{S}_0\tau\sum_{p=1}^{N}\theta_p\mathcal{G}_{p,1}(t)+\mathbb{I}_0\tau\sum_{p=1}^{N}\alpha_p\mathcal{G}_{p,1}(t)\sum_{p=1}^{N}\theta_p\mathcal{G}_{p,1}(t)+\mathbb{S}_0\tau\left(\sum_{p=1}^{N}\theta_p\mathcal{G}_{p,1}(t)\right)^2\right.\\ \left.+\tau\sum_{p=1}^{N}\alpha_p\mathcal{G}_{p,1}(t)\left(\sum_{p=1}^{N}\theta_p\mathcal{G}_{p,1}(t)\right)^2\right]+(\varepsilon_1+\rho+\eta)\mathbb{S}_0+(\varepsilon_1+\rho+\eta)\sum_{p=1}^{N}\alpha_p\mathcal{G}_{p,1}(t).\end{cases} \tag{7.20}$$

Let

$$\Phi_{2,j}=\begin{cases}\frac{t}{N\Gamma(1-\delta)}\sum_{s=1}^{N}\sum_{p=1}^{N}\theta_p\tilde{\psi}_p(\vartheta_s)(t-\vartheta_s)^{-\delta}-\theta(1+\tau\mathbb{I}_0)\times\\ \left(\mathbb{I}_0\mathbb{S}_0+\mathbb{I}_0\sum_{p=1}^{N}\alpha_p\mathcal{G}_{p,1}(t)+\mathbb{S}_0\sum_{p=1}^{N}\theta_p\mathcal{G}_{p,1}(t)+\sum_{p=1}^{N}\alpha_p\mathcal{G}_{p,1}(t)\sum_{p=1}^{N}\theta_p\mathcal{G}_{p,1}(t)\right)\\ +\theta\left[\mathbb{I}_0\mathbb{S}_0\tau\sum_{p=1}^{N}\theta_p\mathcal{G}_{p,1}(t)+\mathbb{I}_0\tau\sum_{p=1}^{N}\alpha_p\mathcal{G}_{p,1}(t)\sum_{p=1}^{N}\theta_p\mathcal{G}_{p,1}(t)+\mathbb{S}_0\tau\left(\sum_{p=1}^{N}\theta_p\mathcal{G}_{p,1}(t)\right)^2\right.\\ \left.+\tau\sum_{p=1}^{N}\alpha_p\mathcal{G}_{p,1}(t)\left(\sum_{p=1}^{N}\theta_p\mathcal{G}_{p,1}(t)\right)^2\right]+(\varepsilon_2+\rho+\varphi)\mathbb{E}_0+(\varepsilon_2+\rho+\varphi)\sum_{p=1}^{N}\theta_p\mathcal{G}_{p,1}(t).\end{cases} \tag{7.21}$$

Let

$$\Phi_{3,j} = \frac{t}{N\Gamma(1-\delta)} \sum_{s=1}^{N} \sum_{p=1}^{N} \lambda_p \tilde{\psi}_p(\vartheta_s)(t-\vartheta_s)^{-\delta} - \varphi\mathbb{E}_0 - \varphi\left(\sum_{p=1}^{N} \theta_p \mathcal{G}_{p,1}(t)\right) + (\lambda+\epsilon+\rho+\varepsilon_3)\mathbb{I}_0 + (\lambda+\epsilon+\rho+\varepsilon_3)\left(\sum_{p=1}^{N} \lambda_p \mathcal{G}_{p,1}(t)\right). \tag{7.22}$$

Let

$$\Phi_{4,j} = \frac{t}{N\Gamma(1-\delta)} \sum_{s=1}^{N} \sum_{p=1}^{N} \vartheta_p \tilde{\psi}_p(\vartheta_s)(t-\vartheta_s)^{-\delta} - \varepsilon_3\mathbb{I}_0 - \varepsilon_3\left(\sum_{p=1}^{N} \lambda_p \mathcal{G}_{p,1}(t)\right) + \varepsilon_2\mathbb{E}_0 + \varepsilon_2\left(\sum_{p=1}^{N} \theta_p \mathcal{G}_{p,1}(t)\right) + \varepsilon_1\mathbb{S}_0 + \varepsilon_1\left(\sum_{p=1}^{N} \alpha_p \mathcal{G}_{p,1}(t)\right) + (\rho+\sigma)\mathbb{Q}_0 + (\rho+\sigma)\left(\sum_{p=1}^{N} \vartheta_p \vartheta_{p,1}(t)\right). \tag{7.23}$$

Let

$$\Phi_{5,j} = \frac{t}{N\Gamma(1-\delta)} \sum_{s=1}^{N} \sum_{p=1}^{N} \zeta_p \tilde{\psi}_p(\vartheta_s)(t-\vartheta_s)^{-\delta} - \eta\mathbb{S}_0 - \mathbb{S}_0\left(\sum_{p=1}^{N} \alpha_p \mathcal{G}_{p,1}(t)\right) - \sigma\mathbb{Q}_0 - \sigma\left(\sum_{p=1}^{N} \sigma_p \mathcal{G}_{p,1}(t)\right) - \lambda\mathbb{I}_0 - \lambda\left(\sum_{p=1}^{N} \lambda_p \mathcal{G}_{p,1}(t)\right) + \rho\mathbb{R}_0 + \rho\left(\sum_{p=1}^{N} \zeta_p \mathcal{G}_{p,1}(t)\right). \tag{7.24}$$

The nonlinear algebraic equations in the system presented below are generated by strategically placing nodal points:

$$\Phi_{1,j} = \begin{cases} \frac{t_p}{N\Gamma(1-\delta)} \sum_{s=1}^{N} \sum_{p=1}^{N} \alpha_p \tilde{\psi}_p(\vartheta_s)\left(t_p - \vartheta_s\right)^{-\delta} - B + \theta(1+\tau\mathbb{I}_0) \times \\ \left(\mathbb{I}_0\mathbb{S}_0 + \mathbb{I}_0 \sum_{p=1}^{N} \alpha_p \mathcal{G}_{p,1}(t_p) + \mathbb{S}_0 \sum_{p=1}^{N} \theta_p \mathcal{G}_{p,1}(t_p) + \sum_{p=1}^{N} \alpha_p \mathcal{G}_{p,1}(t_p) \sum_{p=1}^{N} \theta_p \mathcal{G}_{p,1}(t_p)\right) \\ +\theta\left[\mathbb{I}_0\mathbb{S}_0\tau \sum_{p=1}^{N} \theta_p \mathcal{G}_{p,1}(t_p) + \mathbb{I}_0\tau \sum_{p=1}^{N} \alpha_p \mathcal{G}_{p,1}(t_p) \sum_{p=1}^{N} \theta_p \mathcal{G}_{p,1}(t_p)\right. \\ \left. +\mathbb{S}_0\tau\left(\sum_{p=1}^{N} \theta_p \vartheta_{p,1}(t_p)\right)^2 + \tau \sum_{p=1}^{N} \alpha_p \mathcal{G}_{p,1}(t_p)\left(\sum_{p=1}^{N} \theta_p \mathcal{G}_{p,1}(t_p)\right)^2\right] \\ +(\varepsilon_1+\rho+\eta)\mathbb{S}_0 + (\varepsilon_1+\rho+\eta) \sum_{p=1}^{N} \alpha_p \mathcal{G}_{p,1}(t_p) \end{cases}, \tag{7.25}$$

$$\Phi_{2,j} = \begin{cases} \frac{t_p}{N\Gamma(1-\delta)} \sum_{s=1}^{N} \sum_{p=1}^{N} \theta_p \tilde{\psi}_p(\vartheta_s) \left(t_p - \vartheta_s\right)^{-\delta} - \theta(1+\tau\mathbb{I}_0) \times \\ \left(\mathbb{I}_0\mathbb{S}_0 + \mathbb{I}_0 \sum_{p=1}^{N} \alpha_p \mathcal{G}_{p,1}(t_p) + \mathbb{S}_0 \sum_{p=1}^{N} \theta_p \mathcal{G}_{p,1}(t_p) + \sum_{p=1}^{N} \alpha_p \mathcal{G}_{p,1}(t_p) \sum_{p=1}^{N} \theta_p \mathcal{G}_{p,1}(t_p)\right) \\ +\theta\left[\mathbb{I}_0\mathbb{S}_0\tau \sum_{p=1}^{N} \theta_p \mathcal{G}_{p,1}(t_p) + \mathbb{I}_0\tau \sum_{p=1}^{N} \alpha_p \mathcal{G}_{p,1}(t_p) \sum_{p=1}^{N} \theta_p \mathcal{G}_{p,1}(t_p)\right. \\ \left. +\mathbb{S}_0\tau \left(\sum_{p=1}^{N} \theta_p \vartheta_{p,1}(t_p)\right)^2 + \tau \sum_{p=1}^{N} \alpha_p \mathcal{G}_{p,1}(t_p) \left(\sum_{p=1}^{N} \theta_p \mathcal{G}_{p,1}(t_p)\right)^2\right] \\ +(\varepsilon_2 + \rho + \varphi)\mathbb{E}_0 + (\varepsilon_2 + \rho + \varphi) \sum_{p=1}^{N} \theta_p \mathcal{G}_{p,1}(t_p) \end{cases}, \quad (7.26)$$

$$\begin{aligned} \Phi_{3,j} = \frac{t_p}{N\Gamma(1-\delta)} \sum_{s=1}^{N} \sum_{p=1}^{N} \lambda_p \tilde{\psi}_p(\vartheta_s) \left(t_p - \vartheta_s\right)^{-\delta} - \varphi\mathbb{E}_0 - \varphi\left(\sum_{p=1}^{N} \theta_p \mathcal{G}_{p,1}(t_p)\right) \\ + (\lambda + \epsilon + \rho + \varepsilon_3)\mathbb{I}_0 + (\lambda + \epsilon + \rho + \varepsilon_3)\left(\sum_{p=1}^{N} \lambda_p \mathcal{G}_{p,1}(t_p)\right). \end{aligned} \quad (7.27)$$

$$\begin{aligned} \Phi_{4,j} = \frac{t_p}{N\Gamma(1-\delta)} \sum_{s=1}^{N} \sum_{p=1}^{N} \vartheta_p \tilde{\psi}_p(\vartheta_s) \left(t_p - \vartheta_s\right)^{-\delta} - \varepsilon_3\mathbb{I}_0 - \varepsilon_3\left(\sum_{p=1}^{N} \lambda_p \mathcal{G}_{p,1}(t_p)\right) \\ + \varepsilon_2\mathbb{E}_0 + \varepsilon_2\left(\sum_{p=1}^{N} \theta_p \mathcal{G}_{p,1}(t_p)\right) + \varepsilon_1\mathbb{S}_0 + \varepsilon_1\left(\sum_{p=1}^{N} \alpha_p \mathcal{G}_{p,1}(t_p)\right) \\ + (\rho + \sigma)\mathbb{Q}_0 + (\rho + \sigma)\left(\sum_{p=1}^{N} \vartheta_p \mathcal{G}_{p,1}(t_p)\right). \end{aligned} \quad (7.28)$$

Let

$$\begin{aligned} \Phi_{5,j} = \frac{t_p}{N\Gamma(1-\delta)} \sum_{s=1}^{N} \sum_{p=1}^{N} \zeta_p \tilde{\psi}_p(\vartheta_s) \left(t_p - \vartheta_s\right)^{-\delta} - \eta\mathbb{S}_0 - \mathbb{S}_0\left(\sum_{p=1}^{N} \alpha_p \mathcal{G}_{p,1}(t_p)\right) - \sigma\mathbb{Q}_0 \\ - \sigma\left(\sum_{p=1}^{N} \sigma_p \mathcal{G}_{p,1}(t_p)\right) - \lambda\mathbb{I}_0 - \lambda\left(\sum_{p=1}^{N} \lambda_p \mathcal{G}_{p,1}(t_p)\right) + \rho\mathbb{R}_0 \\ + \rho\left(\sum_{p=1}^{N} \zeta_p \mathcal{G}_{p,1}(t_p)\right). \end{aligned} \quad (7.29)$$

Using Broyden's approach, this system can be solved. The Jacobian is given by:

$$\mathbf{J} = \left[J_{jp}\right]_{5N \times 5N} \quad (7.30)$$

The Jacobian can be obtained by evaluating the following partial derivatives.

$$\begin{array}{ccccc}
\frac{\partial \Phi_{1,j}}{\partial \alpha_p}, & \frac{\partial \Phi_{1,j}}{\partial \alpha_p}, & \frac{\partial \Phi_{1,j}}{\partial \alpha_p}, & \frac{\partial \Phi_{1,j}}{\partial \alpha_p}, & \frac{\partial \Phi_{1,j}}{\partial \alpha_p}, \\
\frac{\partial \Phi_{2,j}}{\partial \theta_p}, & \frac{\partial \Phi_{2,j}}{\partial \theta_p}, & \frac{\partial \Phi_{2,j}}{\partial \theta_p}, & \frac{\partial \Phi_{2,j}}{\partial \theta_p}, & \frac{\partial \Phi_{2,j}}{\partial \theta_p}, \\
\frac{\partial \Phi_{3,j}}{\partial \lambda_p}, & \frac{\partial \Phi_{3,j}}{\partial \lambda_p}, & \frac{\partial \Phi_{3,j}}{\partial \lambda_p}, & \frac{\partial \Phi_{3,j}}{\partial \lambda_p}, & \frac{\partial \Phi_{3,j}}{\partial \lambda_p}, \\
\frac{\partial \Phi_{4,j}}{\partial \varrho_p}, & \frac{\partial \Phi_{4,j}}{\partial \varrho_p}, & \frac{\partial \Phi_{4,j}}{\partial \varrho_p}, & \frac{\partial \Phi_{4,j}}{\partial \varrho_p}, & \frac{\partial \Phi_{4,j}}{\partial \varrho_p}, \\
\frac{\partial \Phi_{5,j}}{\partial \sigma_p}, & \frac{\partial \Phi_{5,j}}{\partial \sigma_p}, & \frac{\partial \Phi_{5,j}}{\partial \sigma_p}, & \frac{\partial \Phi_{5,j}}{\partial \sigma_p}, & \frac{\partial \Phi_{5,j}}{\partial \sigma_p}.
\end{array} \tag{7.31}$$

This system's solution yields the values of the α_p's, θ_p's, λ_p's, ϑ_p's, and σ_p's unknown coefficients. By entering α_p's, θ_p's, λ_p's, ϑ_p's, and σ_p's into Eq (7.1), it is possible to calculate the necessary solutions $\mathbb{S}(t), \mathbb{E}(t), \mathbb{I}(t), \mathbb{Q}(t)$ and $\mathbb{R}(t)$ at nodal locations. The experimental rate of convergence, denoted by the formula $r_\varrho(N)$ [54], can be calculated as follows:

$$\mathbf{r}_\varrho(N) = \frac{1}{\log 2} \log \left[\frac{\text{Maximum absolute error at } \frac{N}{2}}{\text{Maximum absolute error at } N} \right]. \tag{7.32}$$

Next we are going to display the graphical results.

7.1. Graphical results

In this section, we present graphical results that showcase the dynamics of various groups of individuals in the fractional order model (3.4). To solve the model numerically, we adopt the method described in [47, 55] and rely on the information provided in Table 1. The resulting figures, which include Figures 4–7, offer valuable insights into the behavior of susceptible ($\mathbb{S}$), exposed ($\mathbb{E}$), infected ($\mathbb{I}$), recovered ($\mathbb{R}$), and quarantined ($\mathbb{Q}$) individuals. Figure 5(a) depicts the fractional-order derivatives of susceptible individuals, which range between 0.50 and 0.90, and shows that the number of susceptible individuals decreases as time progresses due to exposure to the virus. This is a typical behavior observed in other epidemiological models. Figure 5(b) presents the population of exposed individuals, which grows steadily and rapidly as the fractional-order derivative approaches the classical value. This increase is attributed to the higher number of susceptible people becoming infected and joining the exposed class in the initial weeks of the outbreak, suggesting an increased transmission risk during the early stages of the epidemic. The number of infected individuals, depicted in Figure 5(c), increases as the fractional order approaches 1 due to the increased sensitivity of the fractional order. Figure 5(d) illustrates how most students in the confined and infectious stages of the virus leave the exposed class a few weeks after exposure. The exposed population's behavior is identical to that of the population under quarantine, and as the fractional-order derivative becomes closer to the integer order, there are more exposed people overall. The number of recovered individuals is shown in Figure 5(e) and it increases continuously as the fractional-order derivative gets closer to the classical value as a result of the recovery of infected people, which helps to confine the disease. Raising the fractional order will hasten the population increase of the restored class.

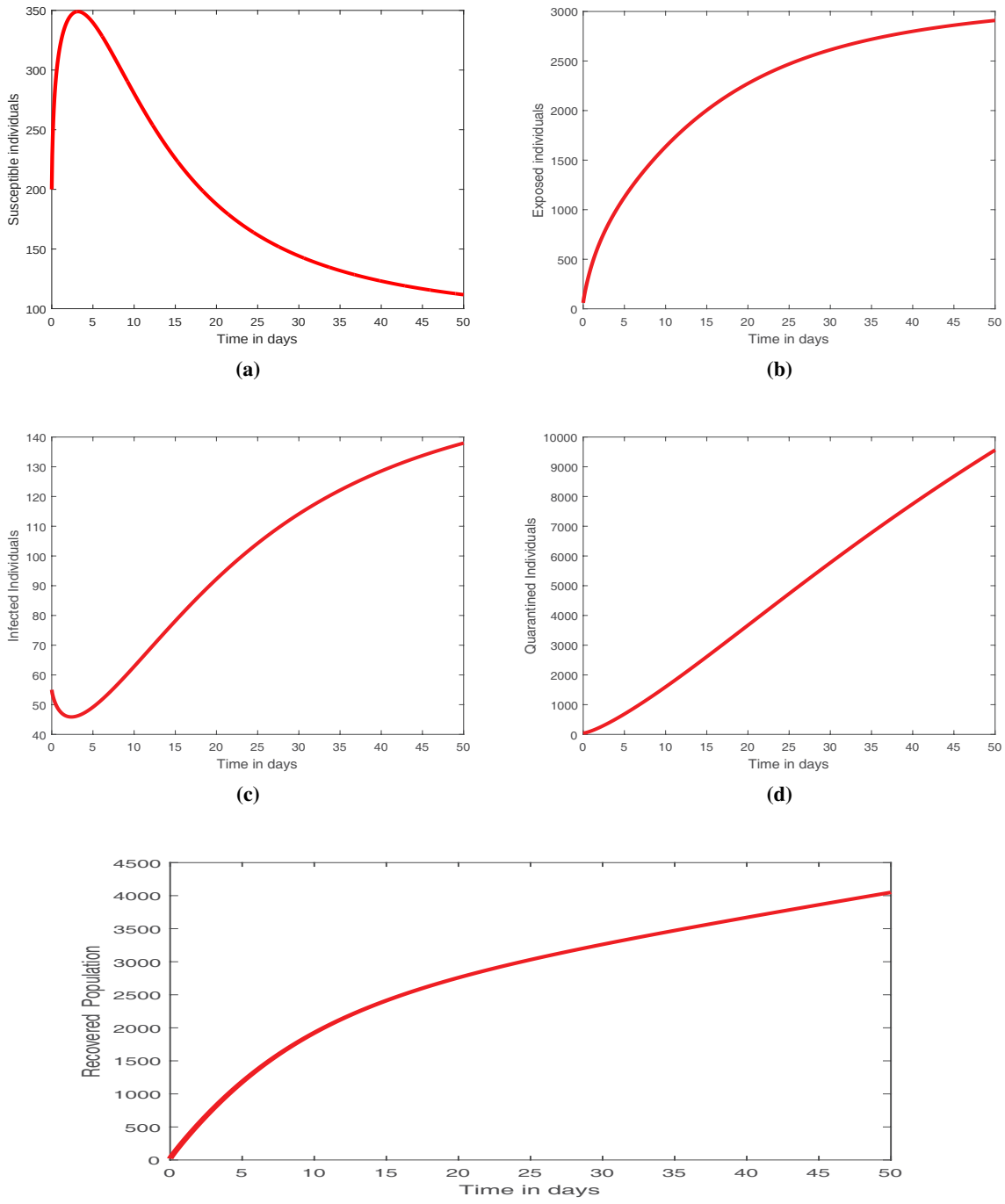

Figure 4. The figure illustrates how the Caputo fractional model responds to different initial conditions, showcasing the behavior of each state variable for a specific value of δ, set at 0.8.

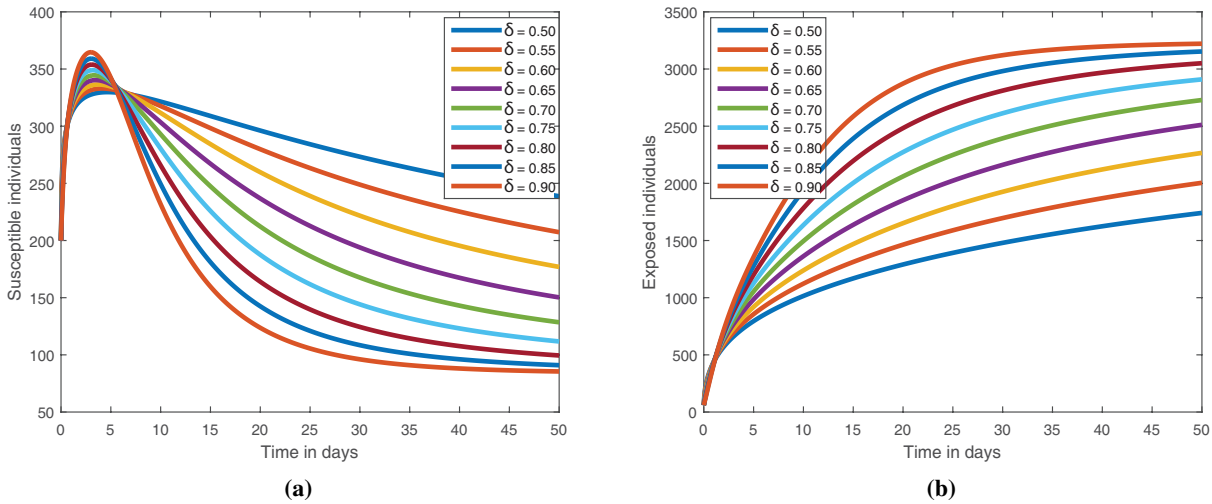

(a)

(b)

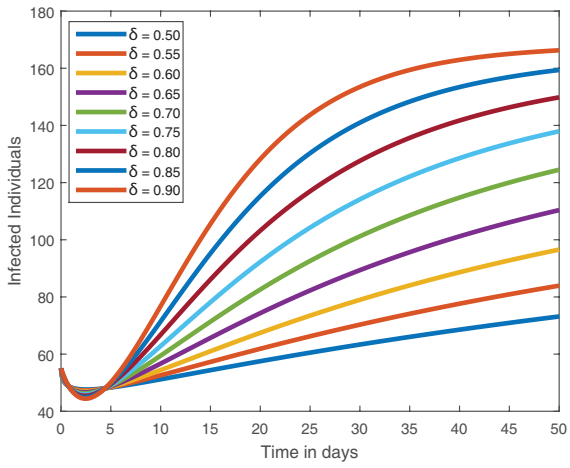

(c)

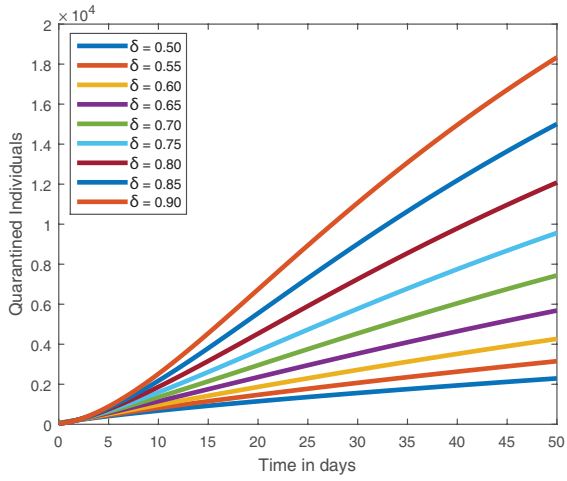

(d)

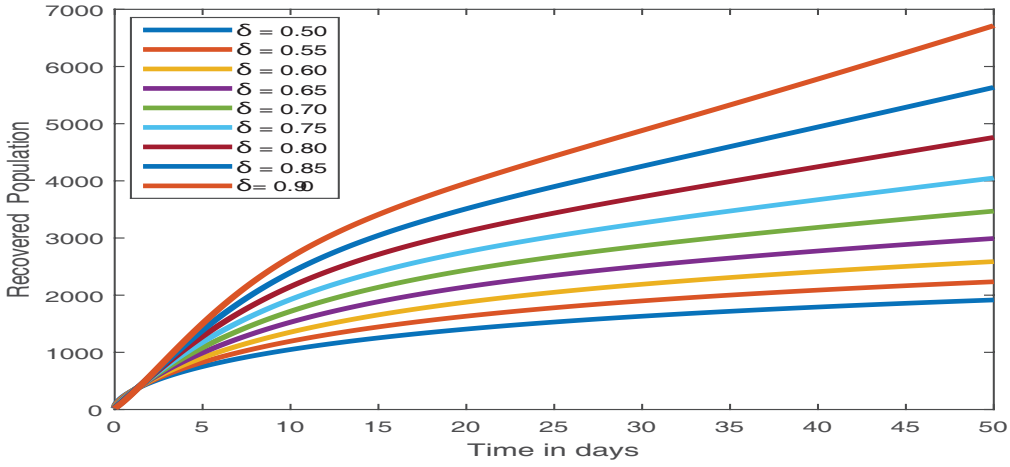

(e)

Figure 5. The figure showcases the distinct behavior of each state variable in the Caputo version of the fractional model, employing the parameter values specified in the graph.

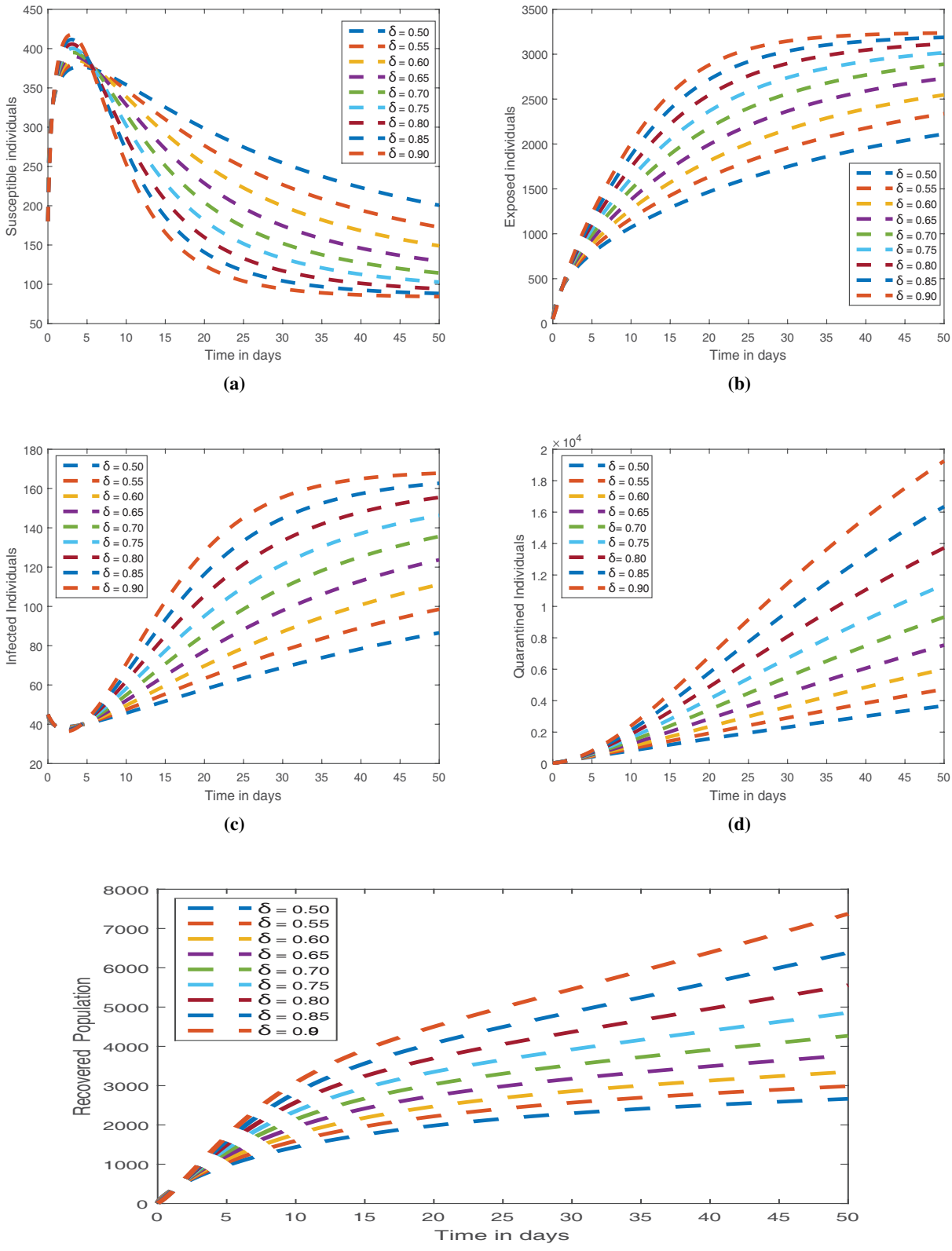

Figure 6. The figure shows the behavior of each state variable for the Caputo fractional model under different initial conditions.

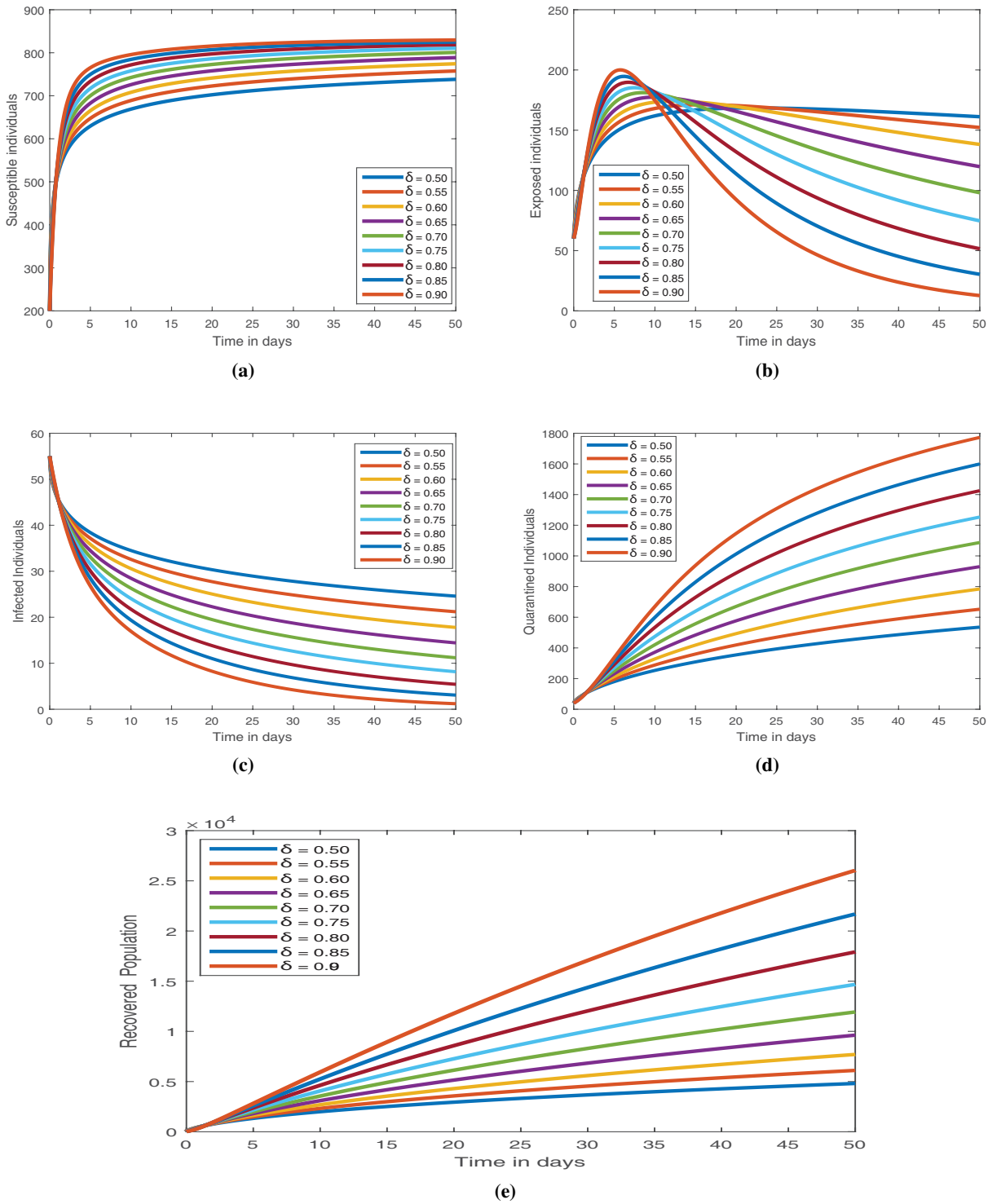

Figure 7. The behavior of each state variable is fully illustrated in this figure for a particular value of the parameter θ, i.e. $\theta = 0.01815$. The y-axis displays the values of the state variables while the x-axis indicates time. Each state variable exhibits a distinct pattern over time in the plot, which clearly illustrates the dynamics of the system. Understanding the basic mechanisms guiding the system and projecting its future behavior under various circumstances are made possible with the use of this information.

8. Conclusions

In conclusion, sensitivity analysis and computational modeling of fractional COVID-19 models by Haar wavelet collocation methods with real data provides valuable insights into the behavior of COVID-19 spread. This method of analysis helps to understand the impact of different variables on the spread of the disease and can be used to make informed decisions about the most effective strategies to mitigate the spread of COVID-19. The use of Haar wavelet collocation methods allows for a more accurate representation of the data, resulting in a more precise and reliable model. This work highlights the importance of using advanced techniques to better understand the dynamics of the COVID-19 pandemic. In this article, we have studied the Covid epidemic model under the fractional derivatives in Caputo sense. The model's existence and uniqueness are established by considering fixed point theory outcomes. To carry out numerical treatment and simulations, we utilize the Haar wavelet collocation method. We also provide parameter estimation for the COVID-19 cases recorded in India from 13 July 2021 to 25 August, 2021. In future, the control parameters may be incorporated into the proposed model by applying optimal control theory to minimize infection among the infected individuals. This would require defining appropriate optimal control variables, as well as Hamiltonian and Lagrangian functions. Another possible modification to the model is to convert it into a stochastic model by introducing a noise term for each class. This could involve incorporating two types of noise: white noise and Levy noise.

Acknowledgments

This research was funded by Deanship of Scientific Research at King Khalid University, Abha, Saudi Arabia, Project under Grant Number RGP.2/27/44. The authors extend their appreciation to the Deanship of Scientific Research at King Khalid University, Abha, Saudi Arabia, for funding this work through the Research Group Project under Grant Number (RGP.2/27/44). The first author appreciates the support provided by Petchra Pra Jom Klao Ph.D. Research Scholarship through grant no (50/2565), by King Mongkut's University of Technology Thonburi, Thailand.

Conflict of interest

The authors declare there is no conflict of interest.

References

1. A. S. Omrani, J. A. Al-Tawfiq, Z. A. Memish, Middle east respiratory syndrome coronavirus (MERS-CoV): Animal to human interaction, pathogens and global health, **109** (2015), 354–362. https://doi.org/10.1080/20477724.2015.1122852
2. World Health Organization, *Weekly epidemiological update on COVID-19—11 January 2023*, 2023. Available from: https://www.who.int/publications/m/item/weekly-epidemiological-update-on-covid-19-11-january-2023

3. M. Z. Tay, C. M. Poh, L. Rénia, P. A. MacAry, L. F. Ng, The trinity of COVID-19: immunity, inflammation and intervention, *Nat. Rev. Immunol.*, **20** (2020), 363–374. https://doi.org/10.1038/s41577-020-0311-8
4. I. Owusu-Mensah, L. Akinyemi, B. Oduro, O. S. Iyiola, A fractional order approach to modeling and simulations of the novel COVID-19, *Adv. Differ. Equations*, **1** (2020), 1–21. https://doi.org/10.1186/s13662-020-03141-7
5. E. Iboi, A. Richardson, R. Ruffin, D. Ingram, J. Clark, J. Hawkins, et al., Impact of public health education program on the novel coronavirus outbreak in the United States, *Front. Public Health*, **9** (2021), 630974. https://doi.org/10.3389/fpubh.2021.630974
6. S. E. Eikenberry, M. Mancuso, E. Iboi, T. Phan, K. Eikenberry, Y. Kuang, et al., To mask or not to mask: Modeling the potential for face mask use by the general public to curtail the COVID-19 pandemic, *Infec. Dis. Modell.*, **5** (2020), 293–308. https://doi.org/10.1016/j.idm.2020.04.001
7. A. Khan, R. Zarin, G. Hussain, N. A. Ahmad, M. H. Mohd, A. Yusuf, Stability analysis and optimal control of covid-19 with convex incidence rate in Khyber Pakhtunkhawa (Pakistan), *Results Phys.*, **20** (2021), 103703. https://doi.org/10.1016/j.rinp.2020.103703
8. P. Veeresha, L. Akinyemi, Fractional approach for mathematical model of Phytoplankton–toxic phytoplankton–zooplankton system with Mittag-Leffler kernel, *Int. J. Biomath.*, **16** (2023), 2250090. https://doi.org/10.1142/S1793524522500905
9. Z. U. A. Zafar, M. Inc, F. Tchier, L. Akinyemi, Stochastic suicide substrate reaction model, *Phys. A*, **610** (2023), 128384. https://doi.org/10.1016/j.physa.2022.128384
10. S. J. Achar, C. Baishya, P. Veeresha, L. Akinyemi, Dynamics of fractional model of biological pest control in tea plants with Beddington–DeAngelis functional response, *Fractal Fractional*, **6** (2021), 1. https://doi.org/10.3390/fractalfract6010001
11. A. Khan, R. Zarin, U. W. Humphries, A. Akgül, A. Saeed, T. Gul, Fractional optimal control of COVID-19 pandemic model with generalized Mittag-Leffler function, *Adv. Differ. Equations*, **1** (2021), 1–22. https://doi.org/10.1186/s13662-021-03546-y
12. M. S. Alqarni, M. Alghamdi, T. Muhammad, A. S. Alshomrani, M. A. Khan, Mathematical modeling for novel coronavirus (COVID-19) and control, *Numer. Methods Partial Differ. Equations*, **38** (2022), 760–776. https://doi.org/10.1002/num.22695
13. A. Khan, R. Zarin, S. Khan, A. Saeed, T. Gul, U. W. Humphries, Fractional dynamics and stability analysis of COVID-19 pandemic model under the harmonic mean type incidence rate, *Comput. Methods Biomech. Biomed. Eng.*, **25** (2022), 619–640. https://doi.org/10.1080/10255842.2021.1972096
14. T. Krueger, K. Gogolewski, M. Bodych, A. Gambin, G. Giordano, S. Cuschieri, et al., Risk assessment of COVID-19 epidemic resurgence in relation to SARS-CoV-2 variants and vaccination passes, *Commun. Med.*, **2** (2022), 23. https://doi.org/10.1038/s43856-022-00084-w
15. A. Calero-Valdez, E. N. Iftekhar, M. Oliu-Barton, R. Böhm, S. Cuschieri, T. Czypionka, et al., Europe must come together to confront omicron, *BMJ*, **376** (2022), o90. https://doi.org/10.1136/bmj.o90

16. R. Markovič, M. Šterk, M. Marhl, M. Perc, M. Gosak, Socio-demographic and health factors drive the epidemic progression and should guide vaccination strategies for best COVID-19 containment, *Results Phys.*, **26** (2021), 104433. https://doi.org/10.1016/j.rinp.2021.104433

17. M. Goyal, H. M. Baskonus, A. Prakash, An efficient technique for a time fractional model of lassa hemorrhagic fever spreading in pregnant women, *Eur. Phys. J. Plus*, **134** (2019), 482. https://doi.org/10.1140/epjp/i2019-12854-0

18. W. Gao, P. Veeresha, D. G. Prakasha, H. M. Baskonus, G. Yel, New approach for the model describing the deathly disease in pregnant women using Mittag-Leffler function, *Chaos Solitons Fractals*, **134** (2020), 109696. https://doi.org/10.1016/j.chaos.2020.109696

19. R. T. Alqahtani, S. Ahmad, A. Akgül, Dynamical analysis of bio-ethanol production model under generalized nonlocal operator in Caputo sense, *Mathematics*, **9** (2021), 2370. https://doi.org/10.3390/math9192370

20. P. Agarwal, R. Singh, Modelling of transmission dynamics of Nipah virus (Niv): A fractional order approach, *Phys. A*, **547** (2020), 124243. https://doi.org/10.1016/j.physa.2020.124243

21. R. Zarin, A. Khan, A. Yusuf, S. Abdel-Khalek, M. Inc, Analysis of fractional COVID-19 epidemic model under Caputo operator, *Math. Methods Appl. Sci.*, **2021** (2021). https://doi.org/10.1002/mma.7294

22. R. Zarin, A. Khan, P. Kumar, Fractional-order dynamics of Chagas-HIV epidemic model with different fractional operators, *AIMS Math.*, **7** (2022), 18897–18924. https://doi.org/10.3934/math.20221041

23. D. Baleanu, A. Fernandez, A. Akgül, On a fractional operator combining proportional and classical differintegrals, *Mathematics*, **8** (2020), 360. https://doi.org/10.3390/math8030360

24. M. Caputo, M. Fabrizio, A new definition of fractional derivative without singular kernel, *Prog. Fractional Differ. Appl.*, **1** (2015), 73–85. http://dx.doi.org/10.12785/pfda/010201

25. A. Atangana, D. Baleanu, New fractional derivatives with nonlocal and non-singular kernel: Theory and application to heat transfer model, preprint, arXiv:1602.03408.

26. P. Agarwal, J. Choi, R. B. Paris, Extended Riemann-Liouville fractional derivative operator and its applications, *J. Sci. Appl.*, **8** (2015), 451–466.

27. R. Zarin, A. Khan, M. Inc, U. W. Humphries, T. Karite, Dynamics of five grade leishmania epidemic model using fractional operator with Mittag–Leffler kernel, *Chaos Solitons Fractals*, **147** (2021), 110985. https://doi.org/10.1016/j.chaos.2021.110985

28. P. Agarwal, J. Choi, Fractional calculus operators and their image formulas, *J. Korean Math. Soc.*, **53** (2016), 1183–1210. https://doi.org/10.4134/JKMS.j150458

29. A. Atangana, Non validity of index law in fractional calculus: A fractional differential operator with Markovian and non-Markovian properties, *Phys. A*, **505** (2018), 688–706. https://doi.org/10.1016/j.physa.2018.03.056

30. D. Kumar, J. Singh, D. Baleanu, A new analysis of the Fornberg-Whitham equation pertaining to a fractional derivative with Mittag-Leffler-type kernel, *Eur. Phys. J. Plus*, **133** (2018), 1–10. https://doi.org/10.1140/epjp/i2018-11934-y

31. D. Kumar, J. Singh, S. D. Purohit, R. Swroop, A hybrid analytical algorithm for nonlinear fractional wave-like equations, *Math. Modell. Nat. Phenom.*, **14** (2019), 304. https://doi.org/10.1051/mmnp/2018063
32. P. Liu, X. Huang, R. Zarin, T. Cui, A. Din, Modeling and numerical analysis of a fractional order model for dual variants of SARS-CoV-2, *Alexandria Eng. J.*, **65** (2023), 427–442. https://doi.org/10.1016/j.aej.2022.10.025
33. R. Zarin, I. Ahmed, P. Kumam, A. Zeb, A. Din, Fractional modeling and optimal control analysis of rabies virus under the convex incidence rate, *Results Phys.*, **28** (2021), 104665. https://doi.org/10.1016/j.rinp.2021.104665
34. A. Atangana, A novel Covid-19 model with fractional differential operators with singular and non-singular kernels: Analysis and numerical scheme based on Newton polynomial, *Alexandria Eng. J.*, **60** (2021), 3781–3806. https://doi.org/10.1016/j.aej.2021.02.016
35. M. U. Rahman, M. Arfan, W. Deebani, P. Kumam, Z. Shah, Analysis of time-fractional Kawahara equation under Mittag-Leffler Power Law, *Fractals*, **30** (2022), 2240021. https://doi.org/10.1142/S0218348X22400461
36. K. Bansal, S. Arora, K. S. Pritam, T. Mathur, S. Agarwal, Dynamics of crime transmission using fractional-order differential equations, *Fractals*, **30** (2022), 2250012. https://doi.org/10.1142/S0218348X22500128
37. K. S. Pritam, T. Mathur, S. Agarwal, Underlying dynamics of crime transmission with memory, *Chaos Solitons Fractals*, **146** (2021), 110838. https://doi.org/10.1016/j.chaos.2021.110838
38. M. Partohaghighi, V. Kumar, A. Akgül, Comparative study of the fractional-order crime system as a social epidemic of the USA scenario, *Int. J. Appl. Comput. Math.*, **8** (2022), 1–17. https://doi.org/10.1007/s40819-022-01399-x
39. M. U. Rahman, S. Ahmad, M. Arfan, A. Akgül, F. Jarad, Fractional order mathematical model of serial killing with different choices of control strategy, *Fractal Fractional*, **6** (2022), 162. https://doi.org/10.3390/fractalfract6030162
40. S. Zhi, L. Y. Deng, J. C. Qing, Numerical solution of differential equations by using Haar wavelets, in *Proceeding of the International Conference on Wavelet Analysis and Pattern Recognition*, (2007), 1037–1044. https://doi.org/10.1109/ICWAPR.2007.4421585
41. K. Shah, Z. A. Khan, A. Ali, R. Amin, H. Khan, A. Khan, Haar wavelet collocation approach for the solution of fractional order COVID-19 model using Caputo derivative, *Alexandria Eng. J.*, **59** (2020), 3221–3231. https://doi.org/10.1016/j.aej.2020.08.028
42. B. Prakash, A. Setia, D. Alapatt, Numerical solution of nonlinear fractional SEIR epidemic model by using Haar wavelets, *J. Comput. Sci.*, **22** (2017), 109–118. https://doi.org/10.1016/j.jocs.2017.09.001
43. D. Kumar, R. P. Agarwal, J. Singh, A modified numerical scheme and convergence analysis for fractional model of Lienard's equation, *J. Comput. Appl. Math.*, **339** (2018), 405–413. https://doi.org/10.1016/j.cam.2017.03.011

44. A. Goswami, J. Singh, D. Kumar, An efficient analytical approach for fractional equal width equations describing hydro-magnetic waves in cold plasma, *Phys. A*, **524** (2019), 563–575. https://doi.org/10.1016/j.physa.2019.04.058
45. M. Caputo, F. Mainardi, A new dissipation model based on memory mechanism, *Pure Appl. Geophys.*, **91** (1971), 134–147. https://doi.org/10.1007/BF00879562
46. Y. Chen, M. Yi, C. Yu, Error analysis for numerical solution of fractional differential equation by Haar wavelets method, *J. Comput. Sci.*, **3** (2012), 367–373. https://doi.org/10.1016/j.jocs.2012.04.008
47. Ü. Lepik, H. Hein, Haar wavelets, in *Haar Wavelets*, Springer, 2014. https://doi.org/10.1007/978-3-319-04295-4
48. P. Van den Driessche, J. Watmough, Reproduction number and sub-threshold endemic equilbria for compartmental models of disease transmission, *Math. Biosci.*, **180** (2002), 29–38. https://doi.org/10.1016/S0025-5564(02)00108-6
49. A. E. Taylor, D. C. Lay, *Introduction to Functional Analysis*, CRC Press, 1958.
50. World Health Organization, https://www.who.int/countries/ind/.
51. Ü Lepik, Numerical solution of differential equations using Haar wavelets, *Math. Comput. Simul.*, **68** (2005), 127–143. https://doi.org/10.1016/j.matcom.2004.10.005
52. S. C. Shiralashetti, R. A. Mundewadi, S. S. Naregal, B. Veeresh, Haar wavelet collocation method for the numerical solution of nonlinear Volterra-Fredholm-Hammerstein integral equations, *Global J. Pure Appl. Math.*, **13** (2017), 463–474.
53. Y. Li, W. Zhao, Haar wavelet operational matrix of fractional order integration and its applications in solving the fractional order differential equations, *Appl. Math. Comput.*, **216** (2010), 2276–2285. https://doi.org/10.1016/j.amc.2010.03.063
54. J. Majak, B. Shvartsman, K. Karjust, M. Mikola, A. Haavajõe, M. Pohlak, On the accuracy of the Haar wavelet discretization method, *Compos. Part B Eng.*, **80** (2015), 321–327. https://doi.org/10.1016/j.compositesb.2015.06.008
55. R. Zarin, H. Khaliq, A. Khan, I. Ahmed, U. W. Humphries, A numerical study based on Haar wavelet collocation methods of fractional-order antidotal computer virus model, *Symmetry*, **15** (2023), 621. https://doi.org/10.3390/sym15030621

AIMS Press